

Conformations of, and Non-covalent Interactions in, binary fluoroalcohol...1,4-dioxane
aggregates: Rotational Spectroscopic and DFT studies

by

Qian Yang

A thesis submitted in partial fulfillment of the requirements for the degree of

Master of Science

Department of Chemistry
University of Alberta

© Qian Yang, 2022

Abstract

Conformations of, and non-covalent interactions in, binary aggregates of 1,1,1,3,3,3-hexafluoro-2-propanol (HFIP) and 1-phenyl-2,2,2-trifluoroethanol (PhTFE) with 1,4-dioxane were investigated. These fluoroalcohols and 1,4-dioxane are common solvents for organic reactions. Rotational spectra of the two fluorinated alcohols and 1,4-dioxane mixtures were measured in a supersonic expansion using a chirped-pulse and a cavity-based Fourier transform microwave spectrometers. Systematic conformational searches were carried out using CREST, a recently developed conformational searching tool by Grimme and co-workers, and the subsequent DFT calculations were used to predict the rotational spectroscopic constants and electric dipole components, as well as relative energies to aid the spectral assignments. One conformer of the HFIP...1,4 dioxane and two conformers of the PhTFE...1,4 dioxane dimer were identified experimentally. The non-covalent interactions involved were further analyzed and visualized using the quantum theory of atoms in molecules (QTAIM), non-covalent interactions (NCI) and symmetric-adapted perturbation theory (SAPT) approaches. New insights into the roles of intra- and intermolecular interactions in the conformational relative stability of the above hydrogen-bonded complexes were extracted based on the experimental and theoretical results. Overall, these studies provide important contributions to understanding how 1,4-dioxane affects the conformational spaces of the fluoroalcohol binding partners.

Preface

This thesis is based on the research I did at the University of Alberta between September 2019 and May 2022. The co-workers' contributions to the research are briefly summarized below.

The study presented in Chapter 3 was published as Q. Yang, F. Xie, T. Lu, N. Bui, W. Jäger, Y. Xu, “Hydrogen Bonding Interactions in the 1,1,1,3,3,3-Hexafluoro-2-Propanol···1,4-Dioxane Complex: Rotational Spectroscopy and Density Functional Theory Calculations”, *J. Mol. Spectrosc.*, **2021**, 376, 111408. I was responsible for the theoretical calculations, data analysis, and completion of the first draft. Dr. F. Xie and N. Bui assisted in the experiments and the introduction part of the draft. Dr. T. Lu assisted in theoretical calculations and data analysis. Professor Y. Xu was the supervisory author, guiding me to complete the paper writing, concept establishment and elaboration. Professor W. Jäger was the supervisory author who provided constructive discussions.

Chapter 4 is based on the published manuscript titled “Conformational Landscape of the Hydrogen-Bonded 1-Phenyl-2,2,2-Trifluoroethanol···1,4-Dioxane Complex: Dispersion Interactions and Conformational Conversion, <https://doi.org/10.1021/acs.jpca.2c01667>” by Qian Yang, Colton D. Carlson, Wolfgang Jäger, Yunjie Xu. I was responsible for the theoretical calculations, data analysis, and preparation of the paper draft. C. D. Carlson assisted in some analyses. Professor Y. Xu was the supervisory author and was involved in the concept formation, data analysis and draft composition. Professor W. Jäger was the supervisory author who did the data collection during the pandemic shutdown period and reviewed the manuscript.

Acknowledgments

I would like to extend my sincerest thanks to my supervisors Yunjie Xu and Wolfgang Jäger who have helped me a lot with my graduate studies. They provided much encouragement and guidance over the past two years. Prof. Xu gave me very good guidance and great help in the microwave experiments and writing of the papers, and she has carefully reviewed and patiently guided many times when I was writing the papers. I am also thankful to Prof. Wolfgang Jäger for helping me with the microwave experiments and the basic theory during the course of my research.

I also would like to thank Dr. Fan Xie and Dr. Tao Lu who help me with my experiments and data analyses. They were very patient in answering my questions and helping me with some technical problems I encountered, especially the python and Linux scripts written by Fan which improved the efficiency of my work so that I could move my research forward..

In addition, I would like to thank my dear friends Arsh, Bowei, Haolu, Mohammad, Mutasem, Guojie, Yanqing and Colton who bring me a lot fun and help me overcome the homesickness. They have given me great care in these two years and filled my youth with the warmth of friendship.

Table of Contents

Chapter 1	1
Introduction.....	1
Chapter 2.....	6
Experimental and Theoretical Details.....	6
2.1 Chirped-pulsed Fourier Transform Microwave (CP-FTMW) Spectrometer.....	6
2.2 Theoretical Calculations	8
2.3 Methods of Analyses.....	10
Chapter 3.....	13
Hydrogen Bonding Interactions in the 1,1,1,3,3,3-Hexafluoro-2-Propanol··1,4-Dioxane Complex: Rotational Spectroscopy and Ab Initio Calculations	13
3.1 Introduction.....	14
3.2 Results and Discussion	15
3.2.1 Conformational Searches	15
3.2.2 Spectroscopic Analyses and Conformational Assignment	17
3.2.3 Conformational Conversion and Binding Strength.....	19
3.3 Conclusions.....	23
3.4. Experimental and Computational Details	23
Chapter 4.....	28
Conformational Landscape of the Hydrogen-Bonded 1-Phenyl-2,2,2-Trifluoroethanol··1,4- Dioxane Complex: Dispersion Interactions and Conformational Conversion	28
4.1 Introduction.....	29
4.2 Results and Discussion	30
4.2.1 Conformational searches of PhTFE-1,4 dioxane	30
4.2.2 Spectroscopic Assignments of PhTFE-1,4 dioxane.....	32
4.2.3 Conformational conversion.....	34
4.2.4 The role of dispersion interactions.....	37
4.3 Conclusion	40
4.4 Experimental and computational Methods	40
Chapter 5.....	44
Conclusions and Future Work	44

Bibliography	46
Appendix A.....	51
Supporting Information for Chapter 3	51
Appendix B.....	62
Supporting Information for Chapter 4	62

List of Tables

Table 3.1. The relative energies, and spectroscopic parameters of the group a) conformers of the HFIP···1,4-dioxane complex	16
Table 3.2. Experimental spectroscopic parameters of the most stable HFIP···1,4-dioxane conformer	18
Table 3.3. Energies from SAPT analyses (in kJ mol ⁻¹).....	22
Table 4.1. Relative energies and spectroscopic parameters of the group a) and b) conformers of the PhTFE···1,4-dioxane complex.....	32
Table 4.2. Experimental spectroscopic parameters of the two most stable PhTFE···1,4-dioxane conformers	34
Table 4.3. The SAPT energy terms (in kJ mol ⁻¹)	39

List of Figures

Figure 1.1 Structures of the HFIP, TFE and PhTFE fluoroalcohols.....	1
Figure 2.1. A schematic diagram of the chirped-pulse FTMW spectrometer.....	7
Figure 2.2. A schematic diagram of the pulse jet expansion	8
Figure 2.3. The workflow for theoretical calculations.....	9
Figure 3.1. Optimized structures of the seven most stable HFIP···1,4-dioxane conformers	16
Figure 3.2. The experimental chirped-pulse rotational spectrum and a simulated stick spectrum of the most stable HFIP···1,4-dioxane conformer	18
Figure 3.3. (a) Results from QTAIM analyses of I, II, III and HFIP dimer	20
Figure 3.4. A one-dimensional potential energy scan.....	22
Figure 4.1 The experimentally observed conformers of HFIP, TFE, and <i>R</i> -PhTFE monomers ..	31
Figure 4.2. Optimized geometries of the six most stable PhTFE···1,4-dioxane conformers	33
Figure 4.3. Experimental rotational spectrum recorded with a mixture of PhTFE+1,4-dioxane in helium using a 2-6 GHz CP-FTMW spectrometer	35
Figure 4.4. (a) One-dimensional, relaxed potential energy scan of PhTFE-1,4-dioxane starting from (a) <i>t</i> Ph-dio II and (b) <i>t</i> Ph-dio I	37
Figure 4.5 (a) QTAIM analyses and (b) NCI isosurfaces of the four representative PhTFE···1,4-dioxane conformers: <i>t</i> Ph-dio I, <i>t</i> Ph-dio II and <i>t</i> Ph-dio III	40

List of Symbols

A, B, C	Rotational constants
$\mu_{a,b,c}$	Electric dipole moment components
ΔD_e	Relative raw dissociation energies
ΔD_0	Relative zero-point energy corrected dissociation energies
$D_J, D_{JK}, D_K, d_1, d_2$	Quartic centrifugal distortion constants
H_{rot}	Rigid rotor Hamiltonian
$P_{a,b,c}$	Angular momentum along principal inertial axes
$I_{a,b,c}$	Moments of inertia along the a-, b-, and c-axes
J	Rotational quantum number
K	Projection of J onto the principal axis
$K_{a,c}$	Quantum number at oblate and prolate limit
H_0	Hamiltonian of the two-level system
μ_{ab}	Transition dipole moment
E	Strength of external electric field
\hbar	Reduced Planck constant
Ω	Driving vector
Θ	Bloch vector

List of Abbreviations

CP-FTMW	Chirped pulse Fourier transform microwave
TTL	Transistor-transistor logic
AWG	Arbitrary wave generator
FID	Free induction decay
TWT	Traveling-wave tube amplifier
OSC	Oscilloscope
DFT	Density functional theory
HF	Hartree-Fock
MP2	Second order Møller-Plesset perturbation
CREST	Conformer-Rotamer Ensemble Sampling Tool
xTB	A tight bonding semiempirical quantum chemical method
D3BJ	Grimme's dispersion correction with Becke Johnson damping
DFT	Density Functional Theory
B3LYP	Becke, 3-parameter, Lee–Yang–Parr, Hybrid functional
QTAIM	Quantum Theory of Atoms in Molecules
NCI	Non-covalent interaction
BCP	Bond critical point
BSSE	Basis set superposition error
ZPE	Zero-point energy
SAPT	Symmetry adapted perturbation theory
RDG	Reduced density gradient
NMR	Nuclear magnetic resonance

Chapter 1

Introduction

In recent years, fluoroalcohols, such as those studied in this thesis, i.e., 1-phenyl-2,2,2-trifluoroethanol (PhTFE) and 1,1,1,3,3,3-hexafluoro-2-propanol (HFIP) (see Figure 1.1), have attracted considerable attention of the scientific community. They have demonstrated some fascinating solvent properties which clearly set them apart from their nonfluorinated analogues. For example, as common solvents for a variety of organic reactions, these fluoroalcohols tend to demonstrate excellent enhancement for reactions such as oxidations [1] and the CH cleavage reactions [2]. In addition, these fluoroalcohols are often used as co-solvents with water in studies of protein folding and unfolding events [3]. Furthermore, they have also been considered as substitutes for other carbohydrate solvents which have larger negative environmental impacts [4].

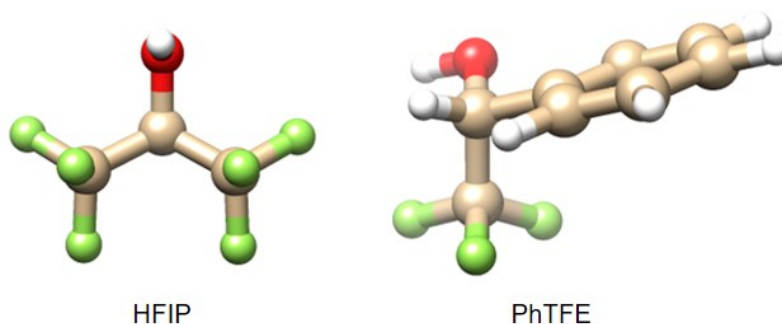


Figure 1.1. The two fluoroalcohol molecules studied in this thesis.

Hamada and his co-workers evaluated the concentration effect of fluoroalcohols on the folding rates of four different proteins and demonstrated that the folding rates of all proteins were increased by the addition of a small amounts of trifluoroethanol [3]. However, the folding rate reached a maximum when the trifluoroethanol concentration was ~5-20%, and further addition of trifluoroethanol resulted in a slowdown in folding. Mulla and his co-workers showed that fluoroalcohols destabilized the exposed hydrophobic side chains in α,α' -*m*-xylylene-*N,N'*-bis-2-phenylpyridinium bromide and stabilized the α -helix. It was hypothesized that fluoroalcohols act synergistically to disrupt water/solute interactions and denature the native structure of proteins [5].

In terms of the strong catalytic effect of fluorinated alcohol solvents, HFIP was recently reviewed as the magical solvent for Pd-catalyzed C-H activation with elevated yield and strong selectivity [2]. Also, HFIP was shown to raise the rate of epoxidation of olefins by hydrogen peroxide by as much as five orders of magnitude when compared to conventional solvents. It was proposed that the strong catalytic activity of HFIP is related to the aggregation-induced enhancement of its hydrogen bond donor capacity and that HFIP aggregates are involved in the main steps of catalysis by Berkessel and co-workers [1]. One proof they carried out is to show that the addition of 1,4-dioxane (a co-solvent for HFIP) results in a significant reduction in the reaction rate [6]. This result was explained because 1,4-dioxane acts as a strong hydrogen bond acceptor and “competes with the active epoxidation pathway”.

Some of the special properties of fluorinated alcohols have been attributed to the high electronegativity and steric and polar effects exhibited by the fluorine atoms [7]. Others have been associated with the hydrogen bonding capability of these fluoroalcohols [1]. Each of these fluoroalcohols contains a OH group which can form hydrogen bond(s) with another molecule. It is therefore important to extract structural information of these fluoroalcohols and evaluate hydrogen bonding interactions among fluoroalcohols and with the mixture of fluoroalcohols and 1,4-dioxanes.

Matuszewicz et al. analyzed the infrared spectrum of HFIP in CCl₄ solution and determined the experimental intensities of the antiperiplanar (ap) and synclinal (sc) conformers by the curve-resolution procedure [8]. While the condensed phase measurements can provide structural information, it is often difficult to extract accurate structural information when the differences are small. It is also difficult to understand or follow how non-covalent interactions affect the preferred conformations of these interesting fluoroalcohols.

Fourier transform microwave (FTMW) spectroscopy, especially chirped pulse (CP)-FTMW spectroscopy [9], has been widely used to probe the structure and energetics of organic molecules and their hydrogen bonded complexes produced in a supersonic jet expansion [10,11,12]. In particular, FTMW spectroscopy can distinguish different conformers with even just minor structural changes for example, different OH orientations. Indeed, conformational distributions of these and other fluoroalcohols have been reported using FTMW spectroscopy [13,14,15]. Furthermore, the OH orientation and other conformational preferences of the isolated

fluoroalcohol molecule can be modified by the hydrogen-bonding interactions in fluoroalcohol aggregates in complexes with water and other molecules [16 , 17 , 18 , 19 , 20 , 21 , 22 , 23,24,25,26,27].

In my graduate research, I focus on applying CP-FTMW spectroscopy, aided by high level theoretical calculations, to probe conformational landscapes of the hydrogen-bonded complexes composed of PhTFE and HFIP with 1,4-dioxane. One point of interest is to examine how such non-covalent interactions modify the conformational preference of these two fluoroalcohols. The dissertation is divided into five chapters. A summary of the contents of each chapter following this one is provided below.

- Chapter 2 briefly discusses the basis of rotational spectroscopy and introduces the broadband chirped pulse FTMW spectrometer which has been utilized in my thesis research. In addition, I also briefly summarize some information related to the electronic structure calculations I performed and the software I used in my research.
- The main research results on HFIP and PhTFE with 1,4-dioxane are provided in Chapters 3 and 4. These two chapters are based on the two research papers which are already published and of which I am the first author.
- Chapter 5 summarizes the main discoveries obtained in this thesis work and provides suggestions of possible work that could be carried out to further enrich the current research.

During my master's studies, I also co-authored a research article: Aran Insausti, Jiarui Ma, Qian Yang, Fan Xie, and Yunjie Xu, "Rotational Spectroscopy of 2-Furoic Acid and Its Dimer: Conformational Distribution and Double Proton Tunneling", *ChemPhysChem*, **2022**, <https://doi.org/10.1002/cphc.202200176>. This work is not included in the current thesis.

References

- [1] A. Berkessel, J. A. Adrio, D. Hüttenhain, J. M. Neudörfl, *J. Am. Chem. Soc.* **2006**, *128*, 8421-8426.
- [2] T. Bhattacharya, A. Ghosha, D. Maiti, *Chem. Sci.*, **2021**, *12*, 3857-3870.

-
- [3] D. Hamada, F. Chiti, J. I. Guijarro, M. Kataoka, N. Taddei, C. M. Dobson, *Nat. Struct. Biol.* **2000**, *7*, 58-61.
- [4] M. Narita, S. Honda, H. Umeyama, S. Obana, *Bull. Chem. Soc. Jpn.* **1988**, *61*, 281-284.
- [5] H. R. Mulla, A. Cammers-Goodwin, *J. Am. Chem. Soc.* **2000**, *122*, 738-739.
- [6] A. Berkessel, J. A. Adrio, *Adv. Synth. Catal.* **2004**, *346*, 275-280.
- [7] P. Shah, A. Westwell, *J. Enzyme Inhib. Med. Chem.* **2007**, *22*, 527-540.
- [8] B. Czarnik-Matuszewicz, S. Pilorz, D. Bienko, D. Michalska, *Vib. Spectrosc.* **2008**, *47*, 44-52.
- [9] G. G. Brown, B. C. Dian, K. O. Douglass, S. M. Geyer, S. T. Shipman, B. H. Pate, *Rev. Sci. Instrum.* **2008**, *79*, 053103.
- [10] C. B. Park, R. W. Field, *J. Chem. Phys.* **2016**, *144*, 200901.
- [11] M. Becucci, S. Melandri, *Chem. Rev.* **2016**, *116*, 5014-5037.
- [12] Y. Xu, J. Van Wijngaarden, W. Jäger, *Inter. Rev. Phys. Chem.* **2005**, *24*, 301-338.
- [13] L.H. Xu, G.T. Fraser, F.J. Lovas, R.D. Suenram, C.W. Gillies, H.E. Warner, J.Z. Gillies, *J. Chem. Phys.* **1995**, *103*, 9541-9548.
- [14] C. D. Carlson, N. A. Seifert, M. Heger, F. Xie, J. Thomas, Y. Xu, *J. Mol. Spectrosc.* **2018**, *351*, 62-67.
- [15] T. Lu, F. Xie, N. A. Seifert, W. Jäger, Y. Xu, *J. Mol. Struct.* **2020**, *1217*, 128359/1-12.
- [16] B. Wu, A. S. Hazrah, N. A. Seifert, S. Oswald, W. Jäger, Y. Xu, *J. Phys. Chem. A* **2021**, *125*, 10401-10409.
- [17] B. Wu, N. A. Seifert, S. Oswald, W. Jäger, Y. Xu, *J. Phys. Chem. A* **2021**, *125*, 5355-5364.
- [18] J. Thomas, I. Peña, C. Carlson, Y. Yang, W. Jäger, Y. Xu, *Phys. Chem. Chem. Phys.* **2020**, *22*, 23019-23027.
- [19] S. Oswald, N. A. Seifert, F. Bohle, M. Gawrilow, S. Grimme, W. Jäger, Y. Xu, *M. A. Suhm, Chem. Int. Ed.* **2019**, *58*, 5080-5084; *Angew. Chem.* **2019**, *131*, 5134-5138.
- [20] N. A. Seifert, J. Thomas, W. Jäger, Y. Xu, *Phys. Chem. Chem. Phys.* **2018**, *20*, 27630-27637.
- [21] W. Huang, J. Thomas, W. Jäger, Y. Xu, *Phys. Chem. Chem. Phys.* **2017**, *19*, 12221-12228.
- [22] J. Thomas, N. A. Seifert, W. Jäger, Y. Xu, *Chem. Int. Ed.* **2017**, *56*, 6289-6293; *Angew. Chem.* **2017**, *129*, 6386-6390.
- [23] J. Thomas, X. Liu, W. Jäger, Y. Xu, *Angew. Chem.* **2015**, *127*, 11877-11881.
- [24] J. Thomas, Y. Xu, *J. Chem. Phys.* **2014**, *140*, 234307/1-5.

-
- [25] J. Thomas, W. Jäger, Y. Xu, *Angew. Chem. Int. Ed.* **2014**, *53*, 7277-7280; *Angew. Chem.* **2014**, *126*, 7405-7408.
- [26] J. Thomas, Y. Xu, *J. Phys. Chem. Lett.* **2014**, *5*, 1850-1855.
- [27] X. Liu, N. Borho, Y. Xu, *Chem. Eur. J.* **2009**, *15*, 270-277.

Chapter 2

Experimental and Theoretical Details

The rotational spectra of all molecular systems I studied were recorded using a CP-FTMW spectrometer whose principles will be briefly described first in section 2.1. In section 2.2, the theoretical calculations used to predict spectroscopic properties of the molecular systems will be outlined. In section 2.3, I will summarize a number of software programs used for analyzing spectral and theoretical results.

2.1 Chirped-pulsed Fourier Transform Microwave (CP-FTMW) Spectrometer

Rotational spectroscopy is a powerful spectroscopic tool for determination of molecular structures in the gas phase. A molecule needs a permanent dipole moment for its pure rotational spectrum to be observed.

The 2-6 GHz Chirped-pulse FTMW spectrometer used [1-3] was constructed based on the design of a 2-8 GHz CP-FTMW spectrometer by Pate and co-workers [4]. It is a broadband spectrometer and improves the detection efficiency compared to the cavity FTMW spectrometer [5,6] which is also available in the laboratory. For example, it would take approximately two weeks to acquire a spectrum over a 4 GHz range using a cavity based FTMW spectrometer with 60 signal averages (accumulation time = 1 minutes) and 0.2 MHz frequency steps, while one single CP-FTMW experiment covers the whole 4 GHz range and typically, several hundred thousand accumulations, which takes about ~6 h, are needed.

A schematic diagram of the CP-FTMW instrument is shown in Figure 2.1. A 12 Gs s⁻¹ arbitrary waveform generator (AWG) is used to generate a 2-6 GHz, 1 μ s long chirped pulse. A traveling-wave tube (TWT) amplifier is used to obtain a chirped pulse of approximately 400 W. Typically, we use only the 100 W experimental setting. The amplified MW pulse is broadcasted using a horn antenna which is situated inside a vacuum chamber. Before, the sample is injected into the chamber as a pulsed jet expansion, arranged perpendicularly to the horn antenna. After the pulsed excitation of the sample, the free induction decay (FID) signal is collected by a receiving

horn antenna and transmitted to a 25 Gs s^{-1} oscilloscope where the signal is digitized in the time domain, accumulated, and then Fourier transformed into the frequency domain signal.

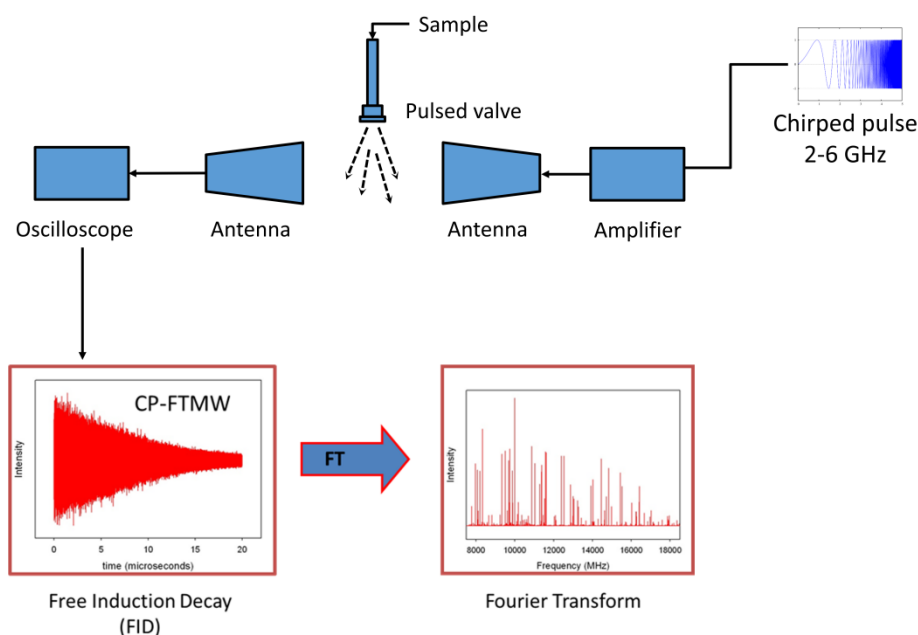


Figure 2.1. A schematic diagram of the chirped-pulse FTMW spectrometer.

Supersonic Jet Expansion: Generally, many rotational levels are populated at room temperature, leading to very low rotational transition intensity. A supersonic jet expansion (Figure 2.2) is utilized to cool molecules to a very low rotational temperature of only a few Kelvins, greatly increasing the line intensity of low J transitions and decreasing spectral congestion. The supersonic expansion beam technology greatly expands the range of accessible molecular systems such as weakly bound molecular clusters, and significantly improves the sensitivity and frequency resolution of rotational spectra detected [7-9].

In a supersonic jet expansion, molecules are mixed with inert gas (usually He or Ne) under a high pressure (typically 1-5 bar), and adiabatically expanded through a pulsed nozzle hole into a vacuum chamber (10^{-6} Torr). After the nozzle is opened, many collisions (mainly with the carrier gas atoms) occur near the nozzle orifice. Only molecules with a particular moving direction can exit the orifice, generating a collision-less molecular beam and leading to an extremely low translational temperature (a few m K). Due to the energy exchange efficiency between the rotational degrees of freedom and the translational degrees of freedom, the molecules are cooled

to a rotational temperature of $\sim 1-4$ K. Therefore, compared with room temperature, the rotation spectrum at low temperature is greatly simplified and intensified.

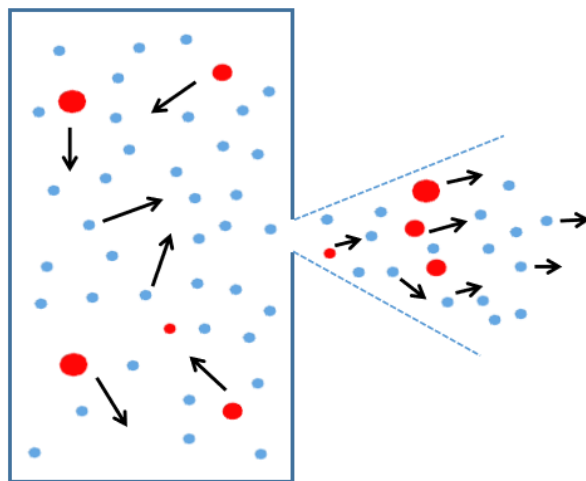


Figure 2.2. A schematic diagram of the pulse jet expansion.

2.2 Theoretical Calculations

Conformation Searches: In general, all species with permanent electric dipole moments can be detected in an FTMW experiment. Therefore, the resulting spectrum usually contains many rotational transitions belonging to multiple species. In order to assign a set of rotational transitions that belong to a particular species, it is very helpful to have the predicted rotational constants and electric dipole moment components and other spectroscopic properties of the species of interest. Furthermore, with many possible conformers, it would be helpful to have some prior knowledge of the relative stability ordering of these conformers.

To search for possible minimum energy structures of molecules, we employed a recently developed computer code named CREST (conformer-rotamer ensemble sampling tool) [10]. This code was built upon the previous semiempirical tight-binding (TB) quantum chemistry method by Grimme and co-workers, called GFN-xTB [11,12]. The new code is designed for fast and reliable exploration and screening of the conformational space of mid- to large-sized molecules with up to about a thousand atoms [13,14]. Besides, GFN-xTB is a new extended semi-empirical tight-binding model that is specifically parameterized for geometry, frequency, and non-covalent molecular interaction energy.

The Workflow of Theoretical Calculations: The workflow for the theoretical calculations is shown in Figure 2.3. First, the input structure drawn is pre-optimized with a cheap forced field method. We then apply CREST to perform molecular dynamics-based (MD) sampling of conformational ensembles. Many molecular structures are generated on the trajectories of MD simulation and are saved and optimized with xTB. Duplicate structures are removed inside CREST. The remaining conformers, ranked by their xTB energies, are included in the CREST conformer ensemble. Often we run CREST multiple times. A script written in the group [15] is used to remove duplicate structures. In this script, $\text{RMSD} = \text{sum of (coordinate difference of all atoms except H)}^2$. $\text{RMSD} = 0$ means that the two structures are identical, while larger RMSD means more unlike conformers. An empirically determined RMSD is set for every system studied. Typically, a value is selected and the resulting geometries are checked to make sure that the structures are not the same as each other. If many structures are the same, we increase the RMSD value to ensure that the output candidates have different geometries. For example, the RMSD values for HFIP...1,4 dioxane and PhTFE...1,4 dioxane are 0.2 \AA^2 and 0.1 \AA^2 , respectively. The final CREST candidates are optimized at the DFT level using the Gaussian electronic structure package [16]. The resulting conformations are arranged according to their relative energies. After that, the predicted spectroscopic constants such as rotational constants and electric dipole moment components of the lowest energy conformers are used to simulate their rotational spectra in order to aid the experimental spectral assignment.

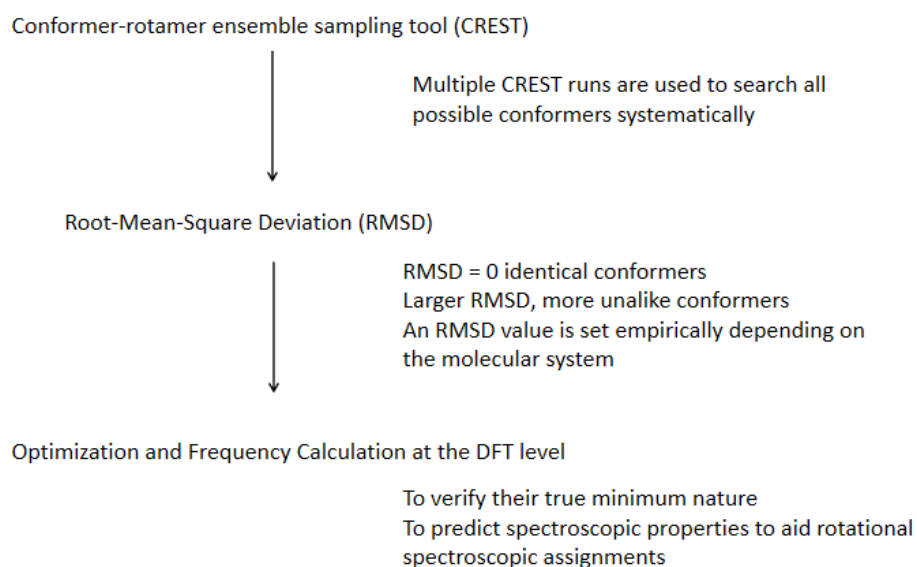


Figure 2.3. The workflow for theoretical calculations.

2.3 Methods of Analyses

The PGOPHER [17] program is used to generate the simulated rotational spectrum and to fit the assigned rotational transitions to a set of rotational spectroscopic constants including centrifugal distortion constants.

The quantum theory of atoms-in-molecules (QTAIM) [18] and non-covalent interactions (NCI) [19] analyses were performed to analyze the non-covalent intermolecular interactions, especially the regions with strong non-covalent attractive interactions. We used the Multiwfn program [20], VMD software [21] and the Chimera software [22] to visualize the QTAIM and NCI results.

In addition, a symmetry-adapted perturbation theory (SAPT) analysis [23] was done at the SAPT2+(3)/aug-cc-pVDZ level using the PSI4 program [24]. This method allows one to decompose the total interaction energy into four parts: electrostatic, induction, dispersion, and exchange-repulsion energies for further informative comparison among the hydrogen-bonded complexes of interest.

References

- [1] C. D. Carlson, N. A. Seifert, M. Heger, F. Xie, J. Thomas, Y. Xu, *J. Mol. Spectrosc.* **2018**, *351*, 62-67.
- [2] F. Xie, X. Ng, N. A. Seifert, J. Thomas, W. Jäger, Y. Xu, *J. Chem. Phys.* **2018**, *149*, 224306.
- [3] F. Xie, N. A. Seifert, M. Heger, J. Thomas, W. Jäger, Y. Xu, *Phys. Chem. Chem. Phys.* **2019**, *21*, 15408-15416.
- [4] C. Pérez, S. Lobsiger, N. A. Seifert, D. P. Zaleski, B. Temelso, G. C. Shields, Z. Kisiel and B. H. Pate, *Chem. Phys. Lett.* **2013**, 1-15.
- [5] Y. Xu, W. Jäger, *J. Chem. Phys.* 1997, *106*, 7968-7980.
- [6] Y. Xu, W. Jäger, *J. Chem. Phys.* 1997, *107*, 4788-4796.
- [7] J. U. Grabow, W. Stahl, *Z Naturforsch.* **1990**, *45A*, 1043-1044.
- [8] J. U. Grabow, W. Stahl, H. Dreizler, *Rev. Sci. Instrum.*, **1996**, *67*, 4072-4084.
- [9] E. Arunan, S. Dev, P. K. Mandal, *Appl. Spectrosc. Rev.*, **2004**, *39*, 131-181.

-
- [10] S. Grimme, *J. Chem. Theory Comput.* **2019**, *15*, 2847-2862.
- [11] S. Grimme, C. Bannwarth, and P. Shushkov, *J. Chem. Theory Comput.* **2017**, *13*, 1989-2009.
- [12] S. Grimme, C. Bannwarth, S. Dohm, A. Hansen, J. Pisarek, P. Pracht, J. Seibert, and F. Neese, *Angew Chem. Int. Ed.* **2017**, *56*, 14763-14769; *Angew. Chem.* **2017**, *129*, 14958-14964.
- [13] F. Xie, M. Fusè, A. S. Hazrah, W. Jäger, V. Barone, Y. Xu, *Angew. Chem. Int. Ed.*, **2020**, *59*, 22427-22430.
- [14] T. Lu, F. Xie, N. A. Seifert, W. Jäger, Y. Xu, *J. Mol. Struct.* **2020**, *1217*, 128359.
- [15] H. Wang, M. Heger, M. H. Al-Jabiri, Y. Xu, 2022, 27, 38/1-19.
<https://doi.org/10.3390/molecules27010038>.
- [16] Gaussian 16, Revision B.01, M. J. Frisch, G. W. Trucks, H. B. Schlegel, G. E. Scuseria, M. A. Robb, J. R. Cheeseman, G. Scalmani, V. Barone, G.A. Petersson, H. Nakatsuji, X. Li, M. Caricato, A. V. Marenich, J. Bloino, B. G. Janesko, R. Gomperts, B. Mennucci, H. P. Hratchian, J. V. Ortiz, A. F. Izmaylov, J. L. Sonnenberg, D. Williams-Young, F. Ding, F. Lipparini, F. Egidi, J. Goings, B. Peng, A. Petrone, T. Henderson, D. Ranasinghe, V. G. Zakrzewski, J. Gao, N. Rega, G. Zheng, W. Liang, M. Hada, M. Ehara, K. Toyota, R. Fukuda, J. Hasegawa, M. Ishida, T. Nakajima, Y. Honda, O. Kitao, H. Nakai, T. Vreven, K. Throssell, J. A. Montgomery Jr., J. E. Peralta, F. Ogliaro, M. J. Bearpark, J. J. Heyd, E. N. Brothers, K. N. Kudin, V. N. Staroverov, T. A. Keith, R. Kobayashi, J. Normand, K. Raghavachari, A. P. Rendell, J. C. Burant, S. S. Iyengar, J. Tomasi, M. Cossi, J. M. Millam, M. Klene, C. Adamo, R. Cammi, J. W. Ochterski, R. L. Martin, K. Morokuma, O. Farkas, J. B. Foresman, D. J. Fox, Gaussian 16, Revision A.03, Gaussian, Inc., Wallingford, CT, 2016
- [17] C. M. Western, *J. Quant. Spectrosc. Radiat. Transf.*, **2017**, *186*, 221-242.
- [18] R. F. W. Bader, *Chem. Rev.* **1991**, *91*, 893-928.
- [19] E. R. Johnson, S. Keinan, P. Mori-Sánchez, J. Contreras-García, A. J. Cohen, W. Yang, *J. Am. Chem. Soc.* **2010**, *132*, 6498-6506.
- [20] T. Lu, F. Chen, *J. Comp. Chem.* **2012**, *33*, 580-592.
- [21] W. Humphrey, A. Dalke, K. Schulten, *J. Mol. Graph.* **1996**, *14*, 33-38.
- [22] E. F. Pettersen, T. D. Goddard, C. C. Huang, G. S. Couch, D. M. Greenblatt, E. C. Meng, T. E. Ferrin, *J. Comp Chem.* **2004**, *25*, 1605-1612.
- [23] T. M. Parker, L. A. Burns, R. M. Parrish, A. G. Ryno, C. D. Sherrill, *J. Chem. Phys.* **2014**, *140*, 094106/1-16.

-
- [24] R. M. Parrish, L. A. Burns, D. G. A. Smith, A. C. Simmonett, A. E. DePrince, III, E. G. Hohenstein, U. Bozkaya, A. Y. Sokolov, R. D. Remigio, R. M. Richard, J. F. Gonthier, A. M. James, H. R. McAlexander, A. Kumar, M. Saitow, X. Wang, B. P. Pritchard, P. Verma, H. F. Schaefer, III, K. Patkowski, R. A. King, E. F. Valeev, F. A. Evangelista, J. M. Turney, T. D. Crawford, C. D. Sherrill, *J. Chem. Theory Comput.* **2017**, *13*, 3185-3197.

Chapter 3

Hydrogen Bonding Interactions in the 1,1,1,3,3,3-Hexafluoro-2-Propanol···1,4-Dioxane Complex: Rotational Spectroscopy and Ab Initio Calculations ^a

^a This study has been published as Q. Yang, F. Xie, T. Lu, N. Bui, W. Jäger, Y. Xu, “Hydrogen Bonding Interactions in the 1,1,1,3,3,3-Hexafluoro-2-Propanol···1,4-Dioxane Complex: Rotational Spectroscopy and Density Functional Theory Calculations”, *J. Mol. Spectrosc.*, **2021**, *376*, 111408.

3.1 Introduction

The high electronegativity and steric and polar effects exhibited by fluorine have been shown to improve bioavailability and enhance binding affinity in biological systems of some fluorinated organic compounds [1,2]. For example, replacement of C-H with C-F facilitates strong electrostatic interactions with other polar groups because the latter is highly polar and less polarizable [3]. Hydrogen bonding interactions involving fluoroalcohols have attracted much recent attention because of their increasing importance in pharmaceutical, agricultural, and industrial fields. 1,1,1,3,3,3-hexafluoro-propan-2-ol, also named hexafluoroisopropanol (HFIP), is one such important fluoroalcohol. HFIP can serve as a co-solvent which denatures or helps stabilizing DNA and proteins [4]. In epoxidation reactions of olefins by hydrogen peroxide, HFIP has been shown to raise the reaction rate by a large factor of 10^5 in comparison to other, conventional solvents [5]. To understand this intriguing “HFIP booster phenomenon”, researchers carried out a range of experimental characterizations using kinetic, NMR, and crystal structure analyses [5,6]. A study by Berkessel and co-workers showed that addition of 1,4-dioxane, a co-solvent to HFIP, in the epoxidation of olefins by hydrogen peroxide resulted in a substantial decrease in the reaction rate [5], in comparison to pure HFIP or to addition of other co-solvents ranging from chloroform, 1,2-dichloroethane, and 1,1,1,3,3,3-hexafluoro-2-propyl-methyl ether (HFIPME). It was hypothesized that HFIP’s strong catalytic activity is related to its strong hydrogen-bond donor ability [6]. The addition of 1,4-dioxane, a hydrogen-bond acceptor, may deactivate HFIP, although the details about the rate determining step in the epoxidation reaction are not fully understood. A further important point that emerges from these studies is that self-aggregation of HFIP may enhance its hydrogen-bond donor ability greatly [6]. It is therefore of interest to study the interaction between HFIP and 1,4-dioxane at the molecular level since other important non-covalent interactions in addition to hydrogen bonding may also play a significant role here.

Fourier transform microwave (FTMW) spectroscopy and in particular chirped-pulse (CP)-FTMW spectroscopy [7] has been utilized extensively in recent years to probe structures and energetics of organic molecules and their complexes generated in a supersonic jet expansion [8,9]. Rotational spectroscopic studies of binary fluoroalcohol complexes [10,11] and larger aggregates, such as trifluoroethanol trimer [12] and 2-fluoroethanol trimer [13] and tetramer [14], address the strength of fluoroalcohols as H-bond donors and acceptors. They also provide insights into the

chemical and structural complexity at the interface between the vapor and bulk phases without the complications associated with the condensed phase. Directly related to the current study is the rotational study of the HFIP monomer [15] and the combined CP-FTMW, FTIR, and Raman investigation of HFIP dimers and trimers [16,17]. In the gas phase, HFIP exists in three conformations that are related to the orientation of the OH group: g' and g (a transiently chiral mirror-imaged pair) and an achiral t -form. Only the t -form was detected experimentally in the FTMW study [15]. For the HFIP dimers, while the achiral tt -form still dominates [16], the subsequent multi-messenger study [17] revealed that the only trimer observed experimentally is made exclusively of three metastable chiral HFIP subunits, i.e. g' and g . The coupling of a pulsed jet expansion with CP-FTMW spectroscopy offers a unique opportunity to follow the development of structure and energetics of $(\text{HFIP})_n \cdots (1,4\text{-dioxane})_m$ clusters step-by-step. It would be particularly interesting to evaluate how the hydrogen-bonding strength between HFIP and 1,4-dioxane varies with the number, n , of HFIP and the number, m , of 1,4-dioxane subunits in a cluster. The current study of their binary adduct is the first step towards this goal.

3.2 Results and Discussion

3.2.1 Conformational Searches

As mentioned above, the HFIP monomer can exist in three configurations associated with the orientation of the OH group: t , g' and g where the latter two are a pair of mirror-images [15,17]. The t configuration is the most stable one in the isolated gas phase [15], while there is evidence that the gauche configurations become preferred as HFIP aggregates [17] or in the condensed liquid phase [6]. For the binary HFIP \cdots 1,4-dioxane complex, CREST runs produced 197 candidates for conformers. These were re-optimized at the B3LYP-D3(BJ)/def2-TZVP level of theory, leading to 17 true minimum structures within a relative energy window of about 41 kJ mol⁻¹. These 17 structures can be roughly grouped into three energy classes: a) 0~7 kJ mol⁻¹, b) 16~24 kJ mol⁻¹, and c) 32~41 kJ mol⁻¹, which are associated with different intermolecular binding topologies. Figure 3.1 shows the seven a) structures where a hydrogen bond is formed between OH of HFIP and O of 1,4-dioxane, labelled with Roman numerals in order of their relative energies. Conformers I, II and III utilize the t configuration of HFIP, whereas IV-VII have HFIP in the t' configuration which is actually a transition state for the HFIP monomer [15-17]. In the five b) structures, the two monomeric subunits are connected by a weak CH (HFIP) \cdots O (1,4-

dioxane) hydrogen bond and other weaker contacts, whereas the group c) structures feature only feeble contacts between CH of 1,4-dioxane and F atoms of HFIP. The calculated relative raw energies, ZPE/BSSE corrected relative energies, ZPE/BSSE corrected binding energies, rotational constants, and electric dipole moment components of the group a) conformers calculated at the B3LYP-D3(BJ)/def2-TZVP level of theory are summarized in Table 1, while the corresponding results for group b) and c) structures are collected in Tables S1 and S2 of Appendix A. Additionally, the atomic coordinates for the group a) conformers are provided in Tables S3-S9 of Appendix A. The principal inertial axis system of I is also given in Figure 3.1.

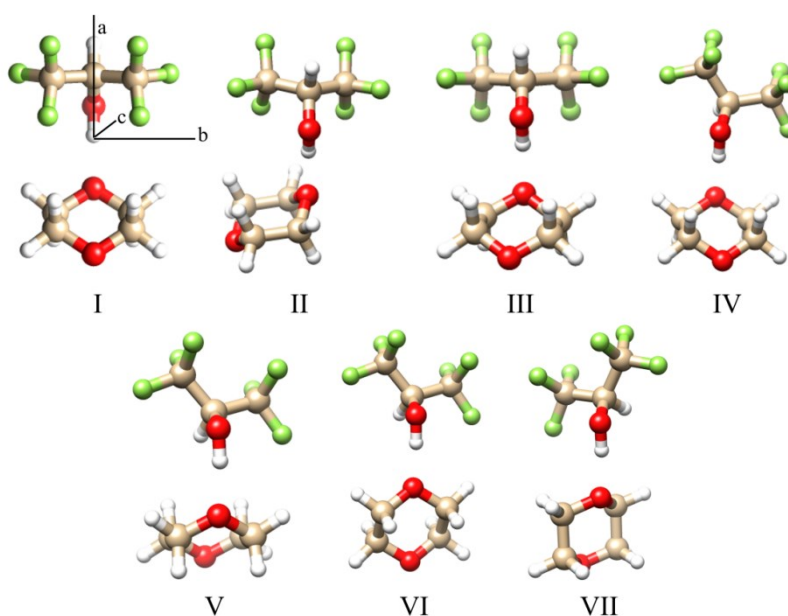


Figure 3.1. Optimized structures of the seven most stable HFIP...1,4-dioxane conformers obtained at the B3LYP-D3(BJ)/def2-TZVP level of theory.

Table 3.1. The relative raw energies, ZPE/BSSE corrected relative energies, ZPE/BSSE corrected binding energies, and spectroscopic parameters of the group a) conformers of the HFIP...1,4-dioxane complex calculated at the B3LYP-D3(BJ)/def2-TZVP level of theory.^a

Conformer	ΔE	ΔE_0	$\Delta E_{0(BSSE)}$	ΔE_b	A	B	C	μ_a	μ_b	μ_c
I	0.0	0.0	0.0	38.0	730	353	295	1.6	0	0.4
II	0.8	0.9	0.8	37.3	792	321	279	1.7	0.4	0.2
III	1.4	1.4	1.5	36.6	796	315	261	1.9	0.1	0.1

IV	3.0	3.0	3.0	39.6	821	269	230	3.7	0.1	2.0
V	4.1	3.8	3.9	38.8	756	308	266	4.4	0.4	0.4
VI	4.6	4.3	4.2	38.5	831	252	217	4.5	0.3	0.9
VII	7.2	6.9	6.8	35.9	946	238	221	4.0	0.6	1.2

^a ΔE , ΔE_0 , $\Delta E_{0(BSSE)}$ are the relative raw, *ZPE* corrected relative, and both *ZPE* and *BSSE* corrected relative energies in kJ mol^{-1} , respectively. ΔE_b is the *ZPE* and *BSSE* corrected binding energy in kJ mol^{-1} . *A*, *B*, and *C* are the rotational constants in MHz and μ_g ($g = a, b, c$) are the electric dipole moment components in Debye.

3.2.2 Spectroscopic Analyses and Conformational Assignment

The rotational spectrum of the most stable conformer was simulated using the predicted rotational constants and electric dipole moment components in Table 1. To aid the assignment of the spectrum of the HFIP \cdots 1,4-dioxane complex, the lines belonging to the HFIP monomer and its ¹³C isotopologues [15] and the dimers and trimer of HFIP [17], the HFIP \cdots water complexes [18] and the HFIP \cdots Ne complex [19] were removed from the broadband CP-FTMW spectrum obtained. The resulting broadband spectrum in the 2 to 6 GHz frequency range is provided in Figure 3.2. We recognized a repeating spectral pattern, consisting of a group of $J+1 \leftarrow J$, *a*-type transitions and obtained a fit for these transitions and tentatively assigned the set of transitions to conformer I. Some weaker *c*-type transitions were then predicted and assigned. No *b*-type transitions could be detected, consistent with the prediction that $\mu_b=0$ for conformer I. After removing lines belonging to the most stable HFIP \cdots 1,4-dioxane conformer, some much weaker, unassigned transitions remain. No other higher energy HFIP \cdots 1,4-dioxane conformers could be assigned. We will discuss the reason for this below.

The set of measured transitions was fitted using Watson’s *A*-reduction [20] semirigid rotor Hamiltonian in its *Ir* representation with the Pgoopher program [21]. The resulting spectroscopic parameters are collected in Table 2. We also summarize the percentage deviations between experimental and predicted rotational constants which are in the order of 1%. The experimental relative electric dipole moment components estimated are also consistent with the relative magnitudes predicted. The magnitudes of the calculated quartic centrifugal distortion constants agree with the related experimental ones. All the evidence supports the assignment of the experimental set of transitions to the most stable binary conformer. The measured transition frequencies are provided in Table S10 of Appendix A.

Table 3.2. Experimental spectroscopic parameters of the most stable HFIP⋯1,4-dioxane conformer.

Parameter	Experiment	Theory (% deviation) ^a
A (MHz)	738.2304(13) ^b	730.2 (1.1%)
B (MHz)	349.17083(64)	352.6 (-1.0%)
C (MHz)	293.49712(59)	295.5 (0.7%)
ΔK (kHz)	-0.733(75)	-1.41
ΔJK (kHz)	0.647(23)	1.41
ΔJ (kHz)	0.0410(32)	0.03
δK (kHz)	0.348(71)	0.68
δJ (Hz)	0.0061(24)	0.0039
μ (D)	$\mu_a \gg \mu_c$, no b -type	1.6/0.0/0.4
σ (kHz)	8.1	N/A
N^d	61	N/A

^a Percentage deviation = 100% x (Exp. -Theo.) / Exp.

^b Errors in parentheses are expressed in units of the least significant digit.

^c σ is the standard deviation of the fit.

^d N is the number of rotational transitions included in the fit.

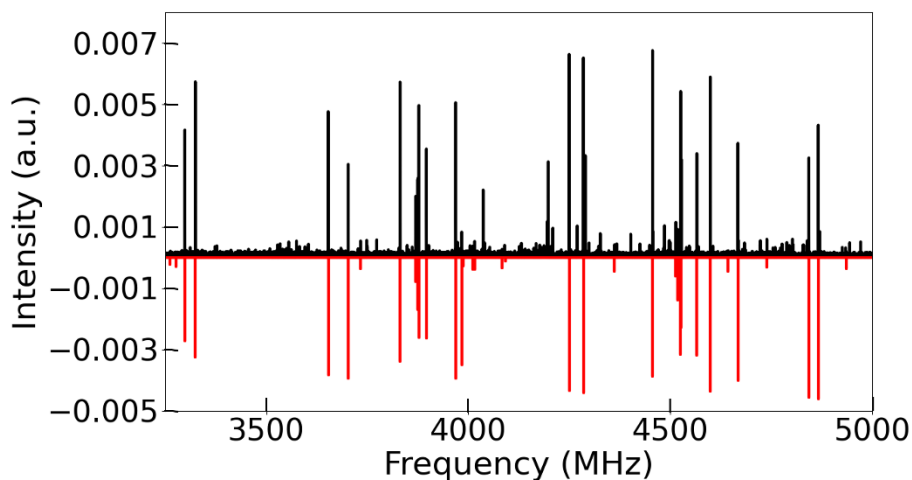


Figure 3.2. The experimental chirped-pulse rotational spectrum (top) and a simulated stick spectrum of the most stable HFIP⋯1,4-dioxane conformer (bottom) using the experimental spectroscopic constants, the permanent electric dipole moment components calculated at the B3LYP-D3(BJ)/def2-TZVP level, and an estimated rotational temperature of 0.5 K. Note that the known experimental transitions of the HFIP monomer, dimers and trimers, the HFIP⋯water complexes and the HFIP⋯Ne complex were removed from the experimental spectrum for clarity.

3.2.3 Conformational Conversion and Binding Strength

As mentioned in the introduction, HFIP is a fluorinated alcohol which can boost the rate of epoxidation of olefins by hydrogen peroxide significantly [5], whereas addition of 1,4-dioxane can almost completely quench the reaction. It was proposed that the epoxidation reactions take place in an HFIP coordination sphere consisting of about 12 HFIP molecules and this coordination sphere provides as much as 5 orders of magnitude of increase in epoxidation rates. Subsequent NMR titration experiments showed that the complexation constant K_C defined as $[\text{complex}] / ([\text{HFIP}] * [\text{ether}])$ is about 33 L mol^{-1} for the HFIP \cdots 1,4-dioxane complex compared to 0.76 L mol^{-1} for the HFIPME \cdots 1,4-dioxane complex. Please note that equilibrium constants are now commonly defined with respect to activity and have no units. This is expected since the latter one has no possibility for H-bond formation. No K_C of the HFIP dimer was reported, which would be valuable for a direct comparison with that of HFIP \cdots 1,4-dioxane to appreciate the competition between the formation of these two highly relevant complexes in the reaction solution.

Below we first focus on the binding strength of the three most stable HFIP \cdots 1,4-dioxane conformers, and then we compare that to the binding strength of the HFIP dimer, as well as two related complexes: HFIP \cdots H₂O and 1,4-dioxane \cdots H₂O. To evaluate and to visualize the intermolecular interactions between HFIP and 1,4-dioxane, we carried out QTAIM analyses and NCI analyses of the electron density distributions of the three most stable HFIP \cdots 1,4-dioxane conformers. The resulting QTAIM bond paths and critical points and the NCI reduced density gradient (RDG) isosurfaces are shown in Figure 3.3 (a) and (b), respectively. In Figure 3.3 (a), structures I, II and III have three, four and two intermolecular bond critical points, respectively. The interaction energies associated with each identified intermolecular bond critical points can be estimated using $E = 0.5 * a_0^3 * V(r)$, where $V(r)$ is the electron potential density at the related bond critical point and a_0 is the Bohr radius [22,23], the corresponding energies are also listed in Figure 3.3 (a). It is found that the O \cdots H hydrogen bond is the dominant attractive interaction in I, II and III, ranging from 54.0 to 58.6 kJ mol^{-1} , considerably stronger than the O \cdots H hydrogen bond ($\sim 30.4 \text{ kJ mol}^{-1}$) in the most stable HFIP dimer. In Figure 3.3 (b), the strong O \cdots H H-bond interactions are visualized as blueish isosurfaces, while the weaker F \cdots H contacts are represented by green isosurfaces.

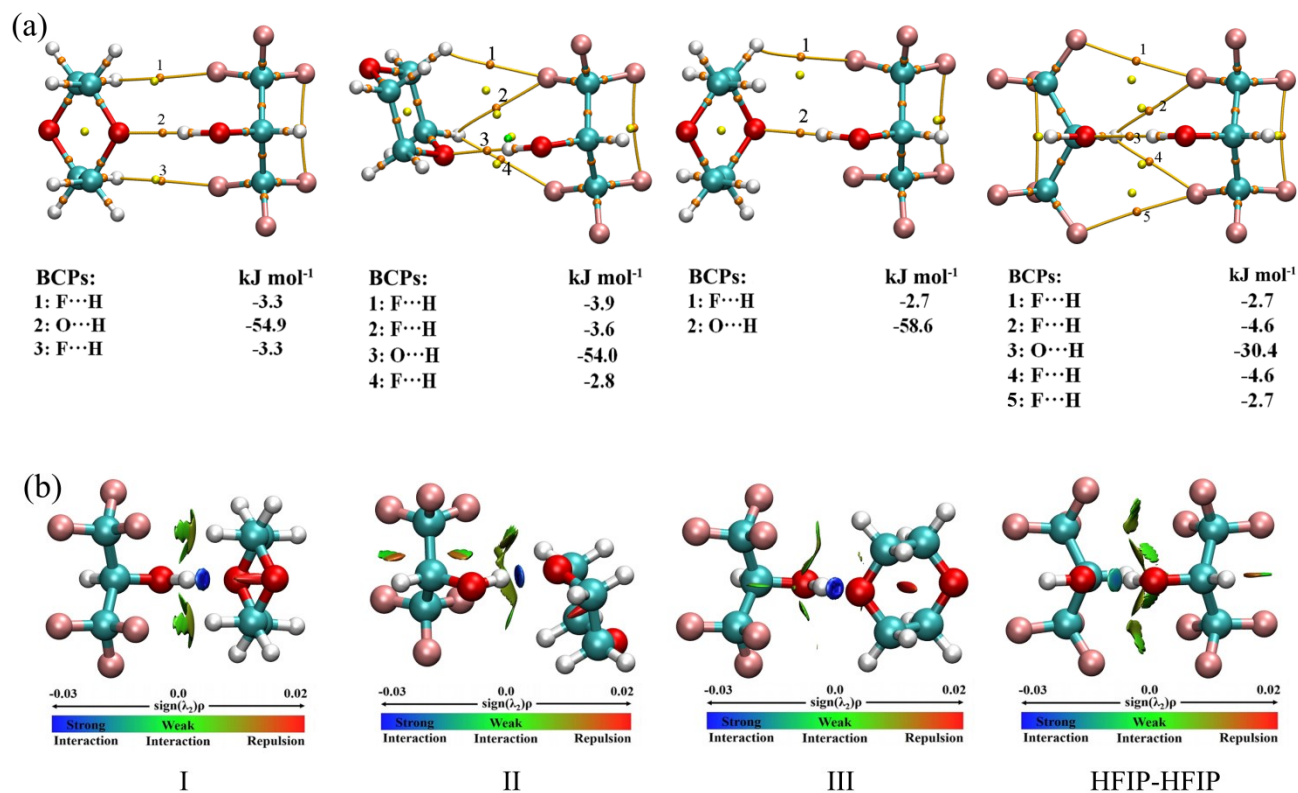


Figure 3.3. (a) Results from QTAIM analyses of I, II, III and HFIP dimer. Orange dots represent the bond critical points, golden lines represent the corresponding bond paths and yellow dots represent ring critical points. (b) Colored NCI isosurfaces of the three most stable HFIP \cdots 1,4-dioxane conformers and the HFIP dimer.

Experimentally, conformer III was not detected even though it is only slightly less stable than structure I which was observed. As one can see from the QTAIM plot and the NCI plot, I and III both feature similarly strong O \cdots H hydrogen bonds and differ only in their weak F \cdots H contacts. While conformer I contains two weak F \cdots H contacts ($\sim 3.3 \text{ kJ mol}^{-1}$), III has only one F \cdots H contact ($\sim 2.7 \text{ kJ mol}^{-1}$). One can imagine that during a supersonic jet expansion, the large number of collisions happening at the nozzle exit may lead to the formation and breaking of this weak F \cdots H contact to convert III to the more stable structure I. This is also consistent with the empirical rule that efficient conformational cooling occurs for conversion barriers of $\leq 4.8 \text{ kJ mol}^{-1}$ [24].

Conformer II, which is also only slightly less stable than I, was not detected either experimentally. In addition to the strong O \cdots H H-bond, II features three weak F \cdots H contacts with interaction energies ranging from ~ 2.8 to 3.9 kJ mol^{-1} . At first glance, one may reason that converting from II to I would require to break all three weak F \cdots H contacts simultaneously. This

would mean that the system needs to overcome a barrier of $\sim 10.3 \text{ kJ mol}^{-1}$, too high to be surmounted in a jet expansion. On the other hand, it was reported before that all these contacts do not need to be broken simultaneously or completely to convert from a high energy conformer to a lower one [25,26]. To verify why structure II was not observed, we carried out a PES scan along a possible interconversion path and the result is shown in Figure 3.4. The PES scan was obtained by varying the dihedral angle Φ (C16-O15-O4-O1) at a step size of 10° starting from conformer III and 36 relaxed single point energy calculations were carried out. The transition state structures were optimized individually, and the harmonic frequency calculations indicate that these transition structures are saddle points with one imaginary frequency. Interestingly, the conformation interconversion barrier from II to I is quite small or non-existent. A closer examination along the conversion path shows that these weak $\text{F}\cdots\text{H}$ contacts remain somewhat intact. Therefore, structure II can completely convert to I in a jet expansion or II may not even be a stable structure because the well supporting it is so shallow.

In addition, we also performed QTAIM and NCI analyses on the most stable HFIP dimer [16,17]. One revealing observation is that the $\text{O}\cdots\text{H}$ bond energy is only 30.4 kJ mol^{-1} , much smaller than the $\text{O}\cdots\text{H}$ bond energies in I, II and III. Clearly, HFIP would favor the formation of the $\text{HFIP}\cdots 1,4\text{-dioxane}$ complex rather than the HFIP dimer when 1,4-dioxane is readily available, thereby preventing the self-aggregation of HFIP, a proposed criterion [5] for the reaction rate enhancement of the epoxidation of olefins by hydrogen peroxide.

To understand the nature of the non-covalent interactions in $\text{HFIP}\cdots 1,4\text{-dioxane}$ more quantitatively, the symmetry-adapted perturbation theory (SAPT) analysis results for the first three most stable $\text{HFIP}\cdots 1,4\text{-dioxane}$ conformers, as well as the results for the related HFIP dimer, the $\text{HFIP}\cdots \text{H}_2\text{O}$ and the $1,4\text{-dioxane}\cdots \text{H}_2\text{O}$ complexes are summarized in Table 3. It is interesting to note that the three most stable $\text{HFIP}\cdots 1,4\text{-dioxane}$ conformers lead substantially in electrostatic, induction, and dispersion attractive interactions over the HFIP dimer, $\text{HFIP}\cdots \text{H}_2\text{O}$ and $1,4\text{-dioxane}\cdots \text{H}_2\text{O}$. These substantially larger attractive energies are partially counter-balanced by considerably larger repulsive exchange energies of these stable $\text{HFIP}\cdots 1,4\text{-dioxane}$ conformers over the other complexes. Overall, these stable $\text{HFIP}\cdots 1,4\text{-dioxane}$ conformers are still about 7.5 to 19.6 kJ mol^{-1} more stable than the other complexes. The above analyses support the conclusion

that the formation of the HFIP···1,4-dioxane complex prevents HFIP to self-aggregate sufficiently to perform its catalytic role in the epoxidation reactions [5,6].

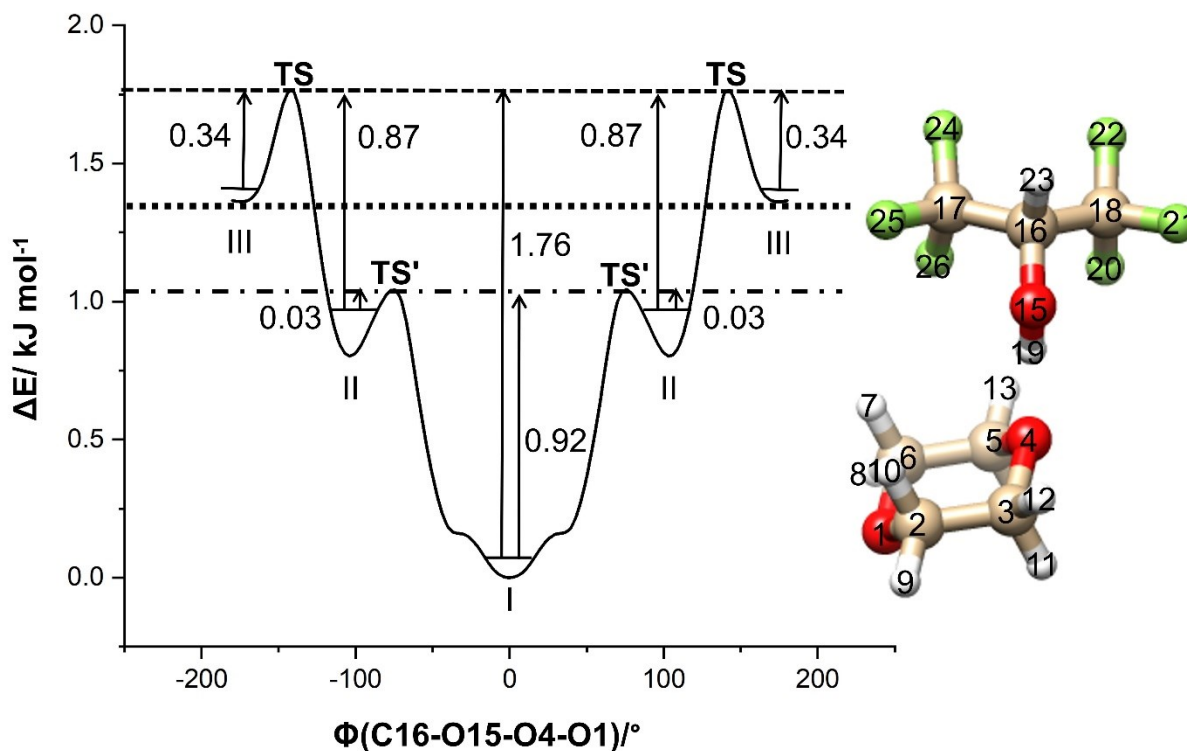


Figure 3.4. A one-dimensional potential energy scan along the dihedral angle Φ (C16-O15-O4-O1) at the B3LYP-D3(BJ)/def2-TZVP level of theory. The *ZPE* corrected barriers (in kJ mol^{-1}) are also indicated. See the main text for details.

Table 3.3. Energies from SAPT analyses (in kJ mol^{-1}) of the three most stable HFIP···1,4-dioxane conformers and related complexes.

Complex	E_{total}	$E_{electrostatic}$	$E_{exchange}$	$E_{induction}$	$E_{dispersion}$
HFIP···1,4-dioxane I	-43.5	-63.1	82.7	-30.2	-32.9
HFIP···1,4-dioxane II	-42.1	-62.6	81.4	-29.4	-31.4
HFIP···1,4-dioxane III	-40.8	-64.8	86.5	-31.7	-30.8
HFIP dimer	-27.1	-35.0	47.9	-15.1	-24.8
HFIP···H ₂ O	-33.3	-61.1	72.7	-24.5	-20.4
1,4-dioxane···H ₂ O	-24.9	-45.9	56.9	-16.6	-19.3

3.3 Conclusions

In summary, the conformational landscape of the HFIP···1,4-dioxane complex was explored using the CREST program where about two hundred candidate structures were identified initially and 17 most stable conformers within a relative energy window of ~ 41 kJ mol⁻¹ were optimized at the B3LYP-D3(BJ)/def2-TZVP level. The experimental rotational spectrum of the HFIP···1,4-dioxane complex revealed one dominant HFIP···1,4-dioxane conformer, corresponding to the most stable structure I, predicted theoretically. The non-observations of conformers II and III in the jet expansion, which are close in energy to I, are explained satisfactorily based on the respective conformational conversion barriers. Further, QTAIM, NCI, and SAPT analyses provide insights into the intermolecular interactions in HFIP···1,4-dioxane and several related complexes, revealing the roles of the stabilizing H-bond and weak F···H contacts in these systems. Analyses of the intermolecular binding energies of HFIP···1,4-dioxane and comparison with the HFIP dimer show that 1,4-dioxane can disrupt HFIP multimer interactions. This is consistent with the notion that HFIP aggregates may be responsible for catalysis of epoxidation reactions and the observation that addition of 1,4-dioxane as co-solvent reduces the reaction rate considerably.

3.4. Experimental and Computational Details

The rotational spectrum of the HFIP···1,4-dioxane complex was recorded with a 2.0–6.0 GHz chirped pulse FTMW spectrometer [27-29] which was constructed based on the design of a 2-8 GHz CP-FTMW spectrometer by Pate and co-workers [7,30]. A 12 Gs s⁻¹ arbitrary waveform generator (AWG) is used to generate a 2-6 GHz, 1 μ s chirped pulse which is amplified using a 400 W traveling wave tube (TWT) amplifier (2.5-7.5 GHz). The amplified MW pulse is broadcasted using a horn antenna which is situated inside a vacuum chamber. Before, the sample is injected into the chamber as a pulsed jet expansion, arranged perpendicularly to the horn antenna. After excitation, the free induction decay (FID) signal is collected by a receiving horn antenna and digitized using a 25 Gs s⁻¹ oscilloscope. For each molecular pulse, the signals from 6 excitation – detection cycles were co-added. In total, about 600k FIDs were averaged and then Fourier transformed to provide the frequency spectrum.

The frequency uncertainty of the measurements is estimated to be ~ 5 kHz and the full width at half height is ~ 125 kHz [31]. HFIP (Sigma Aldrich, 99.9%) was used without further

purification. A mixture of about 0.4% HFIP and 0.4% 1,4-dioxane in Ne (Praxair, 99.999%) at a total pressure of ~30 psi was used for the measurements.

To search for possible minimum energy structures of the HFIP···1,4-dioxane complex, we employed a recently developed computer code named CREST (conformer-rotamer ensemble sampling tool) [32]. This code was built upon the previous semiempirical tight-binding (TB) quantum chemistry method by Grimme and co-workers, called GFN-xTB [33,34]. The new code is designed for fast and reliable exploration and screening of the conformational space of mid- to large-sized molecules with up to about a thousand atoms. It has been successfully applied to support rotational spectroscopic studies of mid-sized organic molecules and their clusters [35,36]. Subsequent geometry optimizations, harmonic frequency calculations, and potential energy surface (PES) scans were completed with the Gaussian 16 suite of programs [37]. The DFT calculations were done with the B3LYP functional [38,39] with dispersion correction (D3) [40] and Becke-Johnson (BJ) damping function [41], and coupled with the def2-TZVP [42,43] basis set. Zero-point energy (*ZPE*) and basis set super position error (*BSSE*) corrections were applied to all energies reported; the *BSSE* corrections were calculated using the counterpoise procedure [44]. We also searched for the transition states along the conformer conversion paths and estimated the corresponding interconversion barriers with respect to the rotation motion of the -OH group of HFIP at the B3LYP-D3(BJ)/def2-TZVP level of theory. Quantum theory of atoms-in-molecules (QTAIM) [46] and non-covalent interactions (NCI) [47] analyses were performed to rationalize the differences in stability among several H-bonded complexes containing either HFIP or 1,4-dioxane for comparison. We used the Multiwfn program [48] and the VMD software [49] to perform and visualize the QTAIM and NCI results. In addition, a symmetry-adapted perturbation theory (SAPT) analysis [50] was done at the SAPT2+(3)/aug-cc-pVDZ level using the PSI4 program [51]. The basis set was chosen based on the recommendation by Sherill and co-workers [错误!未定义书签。]. This method allows one to decompose the total interaction energy into four parts: electrostatic, induction, dispersion, and exchange-repulsion energies for further informative comparison among complexes of interest.

Reference

- [1] P. Shah, A. Westwell, *J. Enzyme Inhib. Med. Chem.* **2007**, *22*, 527-540.
- [2] C. Isanbor, D. O'Hagan, *J. Fluor. Chem.* **2006**, *127*, 303-319.
- [3] J. C. Biffinger, H. W. Kim, S. G. DiMagno, *ChemBioChem* **2004**, *5*, 622-627.
- [4] D.-P. Hong, M. Hoshino, R. Kuboi, Y. Goto, *J. Am. Chem. Soc.* **1999**, *121*, 8427-8433.
- [5] A. Berkessel, J. A. Adrio, *Adv. Synth. Catal.* **2004**, *346*, 275-280.
- [6] A. Berkessel, J. A. Adrio, D. Hgttenhain, J. M. Neudörfl, *J. Am. Chem. Soc.* **2006**, *128*, 8421-8426.
- [7] G. G. Brown, B. C. Dian, K. O. Douglass, S. M. Geyer, S. T. Shipman and B. H. Pate, *Rev. Sci. Instrum.*, **2008**, *79*, 053103.
- [8] C. B. Park, R. W. Field, *J. Chem. Phys.* **2016**, *144*, 200901.
- [9] M. Becucci, S. Melandri, *Chem. Rev.* **2016**, *116*, 5014-5037.
- [10] X. Liu, N. Borho and Y. Xu, *Eur. J. Chem.* **2009**, *15*, 270-277.
- [11] J. Thomas and Y. Xu, *J. Phys. Chem. Lett.* **2014**, *5*, 1850-1855.
- [12] J. Thomas, N. A. Seifert, W. Jäger and Y. Xu, *Angew. Chem. Int. Ed.* **2017**, *56*, 6289-6293.
- [13] J. Thomas, X. Liu, W. Jäger and Y. Xu, *Angew. Chem. Int. Ed.* **2015**, *54*, 11711-11715.
- [14] N. A. Seifert, J. Thomas, W. Jäger, and Y. Xu, *Phys. Chem. Chem. Phys.* **2018**, *20*, 27630-27637.
- [15] A. Shahi, E. Arunan, *J. Phys. Chem. A* **2015**, *119*, 5650-5657.
- [16] S. Oswald, M. A. Suhm, *Angew. Chem. Int. Ed.* **2017**, *56*, 12672-12676.
- [17] S. Oswald, N. A. Seifert, F. Bohle, M. Gawrilow, S. Grimme, W. Jäger, Y. Xu, and M. A. Suhm, *Angew. Chem. Int. Ed.* **2019**, *58*, 5080-5084
- [18] B. Wu, N. A. Seifert, S. Oswald, W. Jäger, Y. Xu, to be submitted.
- [19] B. Wu, N. A. Seifert, S. Oswald, Y. Xu, to be submitted.
- [20] J. K. G. Watson, in: J. R. Durig (Ed.), *Vibrational Spectra and Structure*, vol. 6, Elsevier, New York, 1977, pp. 1-89.
- [21] C. M. Western, *J. Quant. Spectrosc. Radiat. Transf.* **2017**, *186*, 221-242.
- [22] E. Espinosa, E. Molins, C. Lecomte, *Chem. Phys. Lett.* **1998**, *285*, 170-173.
- [23] I. Mata, I. Alkorta, E. Espinosa, E. Molins, *Chem. Phys. Lett.* **2011**, *507*, 185-189.
- [24] R. S. Ruoff, T. D. Klots, T. Emilsson, H. S. Gutowsky, *J. Chem. Phys.* **1990**, *93*, 3142-3150.

-
- [25] J. T. A. Gall, J. Thomas, F. Xie, Z. Wang, W. Jäger, Y. Xu, *Phys. Chem. Chem. Phys.* **2017**, *19*, 29508-29515.
- [26] W. Huang, J. Thomas, W. Jäger, Y. Xu, *Phys. Chem. Chem. Phys.* **2017**, *19*, 12221-12228.
- [27] C. D. Carlson, N. A. Seifert, M. Heger, F. Xie, J. Thomas, Y. Xu, *J. Mol. Spectrosc.* **2018**, *351*, 62-67.
- [28] F. Xie, X. Ng, N. A. Seifert, J. Thomas, W. Jäger, Y. Xu, *J. Chem. Phys.* **2018**, *149*, 224306.
- [29] F. Xie, N. A. Seifert, M. Heger, J. Thomas, W. Jäger, Y. Xu, *Phys. Chem. Chem. Phys.* **2019**, *21*, 15408-15416.
- [30] C. Pérez, S. Lobsiger, N. A. Seifert, D. P. Zaleski, B. Temelso, G. C. Shields, Z. Kisiel and B. H. Pate, *Chem. Phys. Lett.* **2013**, 1-15.
- [31] F. Xie, N. A. Seifert, W. Jäger, Y. Xu, *Angew. Chem. Int. Ed.* **2020**, *59*, 15703-15710.
- [32] S. Grimme, *J. Chem. Theory Comput.* **2019**, *15*, 2847-2862.
- [33] S. Grimme, C. Bannwarth, and P. Shushkov, *J. Chem. Theory Comput.* **2017**, *13*, 1989-2009.
- [34] S. Grimme, C. Bannwarth, S. Dohm, A. Hansen, J. Pisarek, P. Pracht, J. Seibert, and F. Neese, *Angew Chem. Int. Ed.* **2017**, *56*, 14763-14769; *Angew. Chem.* **2017**, *129*, 14958-14964.
- [35] F. Xie, M. Fusè, A. S. Hazrah, W. Jäger, V. Barone, Y. Xu, *Angew. Chem. Int. Ed.* **2020**, *59*, 22427-22430.
- [36] T. Lu, F. Xie, N. A. Seifert, W. Jäger, Y. Xu, *J. Mol. Struct.* **2020**, *1217*, 128359.
- [37] Gaussian 16, Revision B.01, M. J. Frisch, G. W. Trucks, H. B. Schlegel, G. E. Scuseria, M. A. Robb, J. R. Cheeseman, G. Scalmani, V. Barone, G.A. Petersson, H. Nakatsuji, X. Li, M. Caricato, A. V. Marenich, J. Bloino, B. G. Janesko, R. Gomperts, B. Mennucci, H. P. Hratchian, J. V. Ortiz, A. F. Izmaylov, J. L. Sonnenberg, D. Williams-Young, F. Ding, F. Lipparini, F. Egidi, J. Goings, B. Peng, A. Petrone, T. Henderson, D. Ranasinghe, V. G. Zakrzewski, J. Gao, N. Rega, G. Zheng, W. Liang, M. Hada, M. Ehara, K. Toyota, R. Fukuda, J. Hasegawa, M. Ishida, T. Nakajima, Y. Honda, O. Kitao, H. Nakai, T. Vreven, K. Throssell, J. A. Montgomery Jr., J. E. Peralta, F. Ogliaro, M. J. Bearpark, J. J. Heyd, E. N. Brothers, K. N. Kudin, V. N. Staroverov, T. A. Keith, R. Kobayashi, J. Normand, K. Raghavachari, A. P. Rendell, J. C. Burant, S. S. Iyengar, J. Tomasi, M. Cossi, J. M. Millam, M. Klene, C. Adamo, R. Cammi, J. W. Ochterski, R. L. Martin, K. Morokuma, O. Farkas, J. B. Foresman, D. J. Fox, Gaussian 16, Revision A.03, Gaussian, Inc., Wallingford, CT, 2016
- [38] A. D. Becke, *J. Chem. Phys.* **1993**, *98*, 5648-5652.

-
- [39] P. J. Stephens, F. J. Devlin, C. F. Chabalowski, M. J. Frisch, *J. Phys. Chem.* **1994**, *98*, 11623-11627.
- [40] G. Stefan, E. Stephan, G. Lars, *J. Comp. Chem.* **2011**, *32*, 1456-1465.
- [41] A. D. Becke, E. R. Johnson, *J. Chem. Phys.* **2005**, *123*, 154101.
- [42] F. Weigend, R. Ahlrichs, *Phys. Chem. Chem. Phys.* **2005**, *7*, 3297-3305.
- [43] A. Schäfer, C. Huber, R. Ahlrichs, *J. Chem. Phys.* **1994**, *100*, 5829-5835.
- [44] S. F. Boys, F. Bernardi, *Mol. Phys.* **1970**, *19* (4), 553-566.
- [45] C. Peng, H. B. Schlegel, *Isr. J. Chem.* **1993**, *33*, 449-454.
- [46] R. F. W. Bader, *Chem. Rev.* **1991**, *91*, 893-928.
- [47] E. R. Johnson, S. Keinan, P. Mori-Sánchez, J. Contreras-García, A. J. Cohen, W. Yang, *J. Am. Chem. Soc.* **2010**, *132*, 6498-6506.
- [48] T. Lu, F. Chen, *J. Comp. Chem.* **2012**, *33*, 580-592.
- [49] W. Humphrey, A. Dalke, K. Schulten, *J. Mol. Graph.* **1996**, *14*, 33-38.
- [50] T. M. Parker, L. A. Burns, R. M. Parrish, A. G. Ryno, C. D. Sherrill, *J. Chem. Phys.* **2014**, *140*, 094106/1-16.
- [51] R. M. Parrish, L. A. Burns, D. G. A. Smith, A. C. Simmonett, A. E. DePrince, III, E. G. Hohenstein, U. Bozkaya, A. Y. Sokolov, R. D. Remigio, R. M. Richard, J. F. Gonthier, A. M. James, H. R. McAlexander, A. Kumar, M. Saitow, X. Wang, B. P. Pritchard, P. Verma, H. F. Schaefer, III, K. Patkowski, R. A. King, E. F. Valeev, F. A. Evangelista, J. M. Turney, T. D. Crawford, C. D. Sherrill, *J. Chem. Theory Comput.* **2017**, *13*, 3185-3197.

Chapter 4

Conformational Landscape of the Hydrogen-Bonded 1-Phenyl-2,2,2-Trifluoroethanol···1,4-Dioxane Complex: Dispersion Interactions and Conformational Conversion ^a

^a This study has been published by *J. Phys. Chem. A* as Q. Yang, C. D. Carlson, W. Jäger, Y. Xu, “Conformational Landscape of the Hydrogen-Bonded 1-Phenyl-2,2,2-Trifluoroethanol···1,4-Dioxane Complex: Dispersion Interactions and Conformational Conversion”, <https://doi.org/10.1021/acs.jpca.2c01667>.

4.1 Introduction

Fluoroalcohols are commonly used as a co-solvent with water in studies of protein folding and unfolding events because of the high electronegativity and steric and polar effects exhibited by the fluorine atoms [1]. In recent years, fluoroalcohols, such as trifluoroethanol (TFE) and 1,1,1,3,3,3-hexafluoro-2-propanol (HFIP), have attracted considerable attention of the scientific community for their extraordinary assistance in various synthetic transformations [2] including C-H cleavage reactions [3] even though the detailed mechanisms are still not well understood. Berkessel and co-workers hypothesized that HFIP's strong catalytic activity is related to the aggregation-induced hydrogen-bonding enhancement of HFIP, i.e. its increased hydrogen bond donor ability [4]. They showed that in the epoxidation of olefins by hydrogen peroxide, the addition of 1,4-dioxane (a co-solvent for HFIP) results in a significant reduction in the reaction rate [5] because 1,4-dioxane acts as a strong hydrogen bond acceptor and "competes with the active epoxidation pathway" [4].

In the last decade, Fourier transform microwave (FTMW) spectroscopy, especially chirped pulse (CP)-FTMW spectroscopy [6], has been widely used to probe the structure and energetics of organic molecules and their complexes produced in a supersonic jet expansion [7,8]. The significant interest described above, in how non-covalent interactions influence the properties of the mixed solvents containing fluoroalcohols, has inspired researchers to carry out rotational spectroscopic studies of hydrogen-bonded aggregates of fluoroalcohols such as dimers and trimers of mono-fluoroethanol (MFE) [9,10], TFE [11], and HFIP [12,13], as well as their complexes with 1,4-dioxane, such as the HFIP \cdots 1,4-dioxane complex [14]. These studies allow one to examine how the OH orientation and other conformational preferences of an isolated fluoroalcohol molecule are modified by the hydrogen-bonding interactions in the corresponding aggregates. For example, the only HFIP monomeric conformer observed has the *trans* (*t*) OH configuration and is achiral [15] (see Figure 4.1), whereas the most preferred HFIP trimer, which was observed experimentally, consists exclusively of three metastable chiral monomer units, which adopt the *gauche*^{+/-} (*g*^{+/-}) OH configurations [12]. On the other hand, the only HFIP \cdots 1,4-dioxane conformer observed contains the achiral *t*-HFIP conformer [14].

A distinguishing feature of 1-phenyl-2,2,2-trifluoroethanol (PhTFE), compared to TFE and HFIP, is the phenyl substitution (see Figure 4.1). The three conformations of PhTFE are related to the OH orientations, which are *g*⁺, *t*, and *g*⁻. PhTFE is a permanently chiral molecule and the

combinations, $R g^+$ and $R g^-$, are not mirror-imaged to each other, as in the cases of TFE and HFIP. Rather they can be considered as diastereomers to each other. To avoid confusion, we use the R enantiomer of PhTFE throughout the manuscript, consistent with the previous rotational spectroscopic study of the PhTFE monomer where only the g^+ form was observed experimentally [16]. While PhTFE is expected to interact with 1,4-dioxane mainly through an $\text{OH}\cdots\text{O}$ hydrogen bond, similar to $\text{HFIP}\cdots 1,4\text{-dioxane}$ [14], it is of considerable interest to examine how the bulky, phenyl functional group influences the conformational landscape of the $\text{PhTFE}\cdots 1,4\text{-dioxane}$ binary complex.

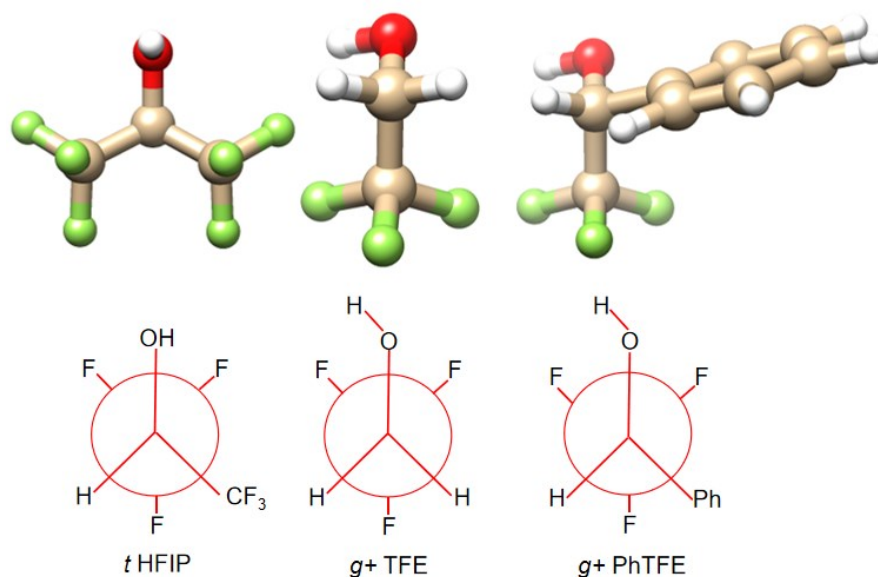


Figure 4.1. The experimentally observed conformers of the HFIP, TFE, and R -PhTFE monomers. The naming is kept the same as in the previous publications for the HFIP [4], TFE [17], and PhTFE [16] monomers. While t HFIP is achiral, g^+ TFE is transiently chiral and the tunneling transitions between the g^+ and g^- TFE were detected [17].

4.2 Results and Discussion

4.2.1 Conformational searches of PhTFE-1,4 dioxane

As previously mentioned, the PhTFE monomer can potentially exist in three conformations that have different OH group orientations: g^+ , t , and g^- , but only g^+ PhTFE was detected experimentally [16]. Although 1,4-dioxane has only one conformation, one may still expect a rich structural diversity of the binary $\text{PhTFE}\cdots 1,4\text{-dioxane}$ complex since the phenyl group may take up many different relative orientations with respect to the 1,4-dioxane ring, in addition to the different OH orientations. The CREST searches and the PES scans produced about 70 candidate

conformers and the subsequent optimizations at the B3LYP-D3(BJ)/def2-TZVP level of theory resulted in a total of 26 conformers. We classify them into three groups with their relative energies in the ranges of: a) 0~3 kJ mol⁻¹, b) 3~8 kJ mol⁻¹, and c) 17~26 kJ mol⁻¹. In group a), the PhTFE subunit takes on the *t*-configuration, while in the two latter ones, either the *g*+ or *g*-PhTFE subunits are used. The calculated rotational constants, electric dipole moment components, relative raw energies, and ZPE/BSSE corrected relative energies, as well as the ZPE/BSSE corrected binding energies of the group a) and b) conformers are listed in Table 4.1, while those of group c) are shown in Table S1 of Appendix B. The atomic coordinates of group a) conformers are provided in Tables S2-S7 of Appendix B. The geometries of the six most stable binary conformers are depicted in Figure 4.2. In the tables and figures below, *t* or *g*+ and *g*-PhTFE are abbreviated as *t*Ph, *g*+Ph, and *g*-Ph, respectively and 1,4-dioxane is denoted as dio.

Table 4.1. Relative energies and spectroscopic parameters of the group a) and b) conformers of the PhTFE···1,4-dioxane complex calculated at the B3LYP-D3(BJ)/def2-TZVP level of theory.^a

Conformer	ΔE	ΔE_0	$\Delta E_{0(BSSE)}$	ΔE_b	<i>A</i>	<i>B</i>	<i>C</i>	μ_a	μ_b	μ_c
<i>t</i> Ph-dio I	0.0	0.0	0.0	38.9	575	294	237	4.1	1.0	0.6
<i>t</i> Ph-dio II	0.7	0.7	0.4	38.5	547	280	216	3.4	2.1	1.5
<i>t</i> Ph-dio III	1.0	0.9	0.6	38.3	524	293	226	3.8	2.1	0.3
<i>t</i> Ph-dio IV	1.0	1.0	0.9	40.2	603	282	229	3.9	1.2	1.1
<i>t</i> Ph-dio V	3.0	2.9	2.8	36.1	607	259	213	4.2	1.4	0.7
<i>g</i> -Ph-dio VI	2.0	3.0	3.6	36.0	496	368	277	2.6	1.4	0.1
<i>g</i> -Ph-dio VII	3.0	3.8	4.4	35.2	450	384	269	1.1	-2.7	-0.1
<i>g</i> +Ph-dio VIII	4.8	4.1	3.7	35.2	723	211	186	-1.0	1.0	-1.6
<i>g</i> -Ph-dio IX	4.2	4.3	4.2	37.2	599	265	210	0.1	2.4	-0.4
<i>g</i> +Ph-dio X	5.5	4.6	4.5	34.7	680	225	203	1.7	-1.9	-0.5
<i>g</i> -Ph-dio XI	4.1	4.8	5.2	39.3	521	316	241	2.5	-2.0	0.3
<i>g</i> -Ph-dio XII	4.5	5.1	5.3	38.7	509	320	233	2.2	2.3	-0.5
<i>g</i> +Ph-dio XIII	7.2	6.0	5.2	34.1	762	186	168	-1.9	-1.8	0.9
<i>g</i> -Ph-dio XIV	6.5	7.1	7.1	38.7	547	295	239	-2.6	1.9	0.1
<i>g</i> +Ph-dio XV	8.2	7.1	6.7	32.1	946	175	169	-1.4	1.1	-1.3
<i>g</i> +Ph-dio XVI	8.5	7.3	7.1	31.7	930	190	181	1.0	1.0	1.5
<i>g</i> -Ph-dio XVII	8.1	7.9	7.4	35.4	557	258	203	1.0	-2.1	0.1

^aThe conformational numbering, I to XVII, is based on the ΔE_0 ordering from low to high. ΔE , ΔE_0 , $\Delta E_{0(BSSE)}$ are the relative raw, *ZPE* corrected relative, and both *ZPE* and *BSSE* corrected relative energies in kJ mol^{-1} , respectively. ΔE_b is the *ZPE* and *BSSE* corrected binding energy in kJ mol^{-1} . *A*, *B*, and *C* are the rotational constants in MHz and $\mu_{a,b,c}$ are the electric dipole moment components in Debye.

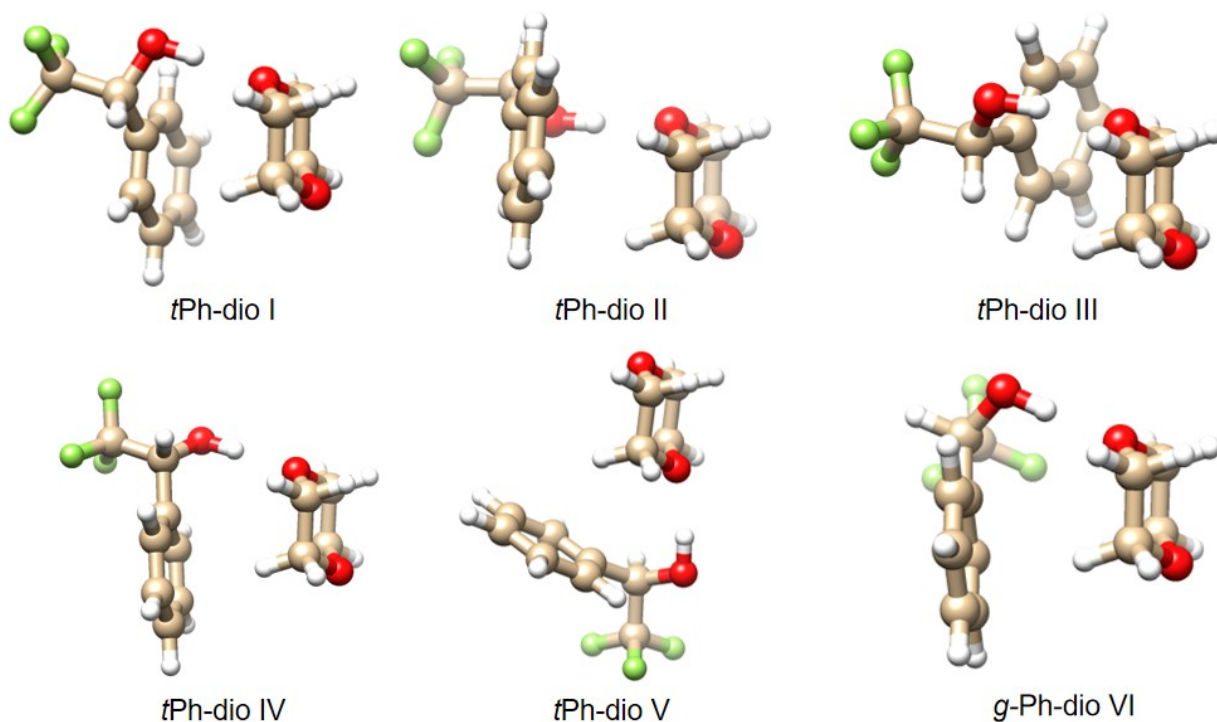


Figure 4.2. Optimized geometries of the six most stable PhTFE...1,4-dioxane conformers obtained at the B3LYP-D3(BJ)/def2-TZVP level of theory.

4.2.2 Spectroscopic Assignments of PhTFE-1,4 dioxane

After removing the known transitions of the PhTFE monomer and its ^{13}C isotopologues [错误!未定义书签。], as well as those of PhTFE...water [18] from the experimental spectrum, a set of *a*-type transitions was recognized straightforwardly and assigned based on the simulated spectrum of *tPh-dio* I using the spectroscopic constants listed in Table 4.1. Subsequently, the weaker *b*- and much weaker *c*-type transitions were also assigned. The final spectroscopic fit of rotational parameters was carried out using Watson's A-reduction [19] semirigid rotor Hamiltonian in its Ir representation with the Pgoopher program [20]. Indeed, the good agreement between the

experimental and theoretical rotational constants and relative electric dipole components allowed us to confidently assigned the carrier to *t*Ph-dio I.

There were a number of much weaker transitions left after subtracting those of *t*Ph-dio I from the spectrum. After considerable trying, we were able to assign another set of transitions. The same spectroscopic fitting procedure was applied. The resulting rotational constants and relative electric dipole moment components indicate that the carrier is *t*Ph-dio II. All measured transition frequencies of *t*Ph-dio I and *t*Ph-dio II are tabulated in Tables S8 and S9 of Appendix B, respectively. The resulting spectroscopic parameters are collected in Table 4.2. The theoretical rotational constants deviate by 0.1% ~ 1.5% for *t*Ph-dio I and ~1.2% to 2.1% for *t*Ph-dio II from the experimental ones. The difference of rotational constants between *t*Ph-dio I and *t*Ph-dio II are 3.9%, 6.9% and 11.4%, considerably larger than the deviation between the experimental and theoretical rotational constants indicated above, allowing one to differentiate these two conformers confidently. The experimental spectrum is compared with the simulated spectra of the two assigned binary conformers in the frequency range of 3.25 to 5.90 GHz in Figure 4.3.

Table 4.2. Experimental spectroscopic parameters of the two most stable PhTFE···1,4-dioxane conformers.

Parameter	<i>t</i> Ph-dio I	<i>t</i> Ph-dio II
<i>A</i> (MHz)	574.17852(94) ^a	553.54009(76) ^a
<i>B</i> (MHz)	289.19763(52)	274.60731(68)
<i>C</i> (MHz)	233.48278(35)	212.61151(37)
Δ_K (kHz)	0.2100(32)	0.1932(59)
Δ_{JK} (kHz)	-0.0490(54)	-0.0039(18)
Δ_J (kHz)	0.0288(53)	0.0251(26)
δ_K (kHz)	0.0064(04)	0.0377(19)
δ_J (kHz)	0.0064(44)	0.0061(67)
μ ^b	$\mu_a \gg \mu_b > \mu_c$	$\mu_a > \mu_b > \mu_c$
σ (kHz) ^c	7.5	8.7
<i>N</i> ^c	171	156

^a Errors in parentheses are expressed in units of the least significant digit.

^b Relative magnitudes of the electric dipole moment components estimated based on the experimental transition intensity.

^c σ is the standard deviation of the fit and *N* is the number of rotational transitions included in the fit.

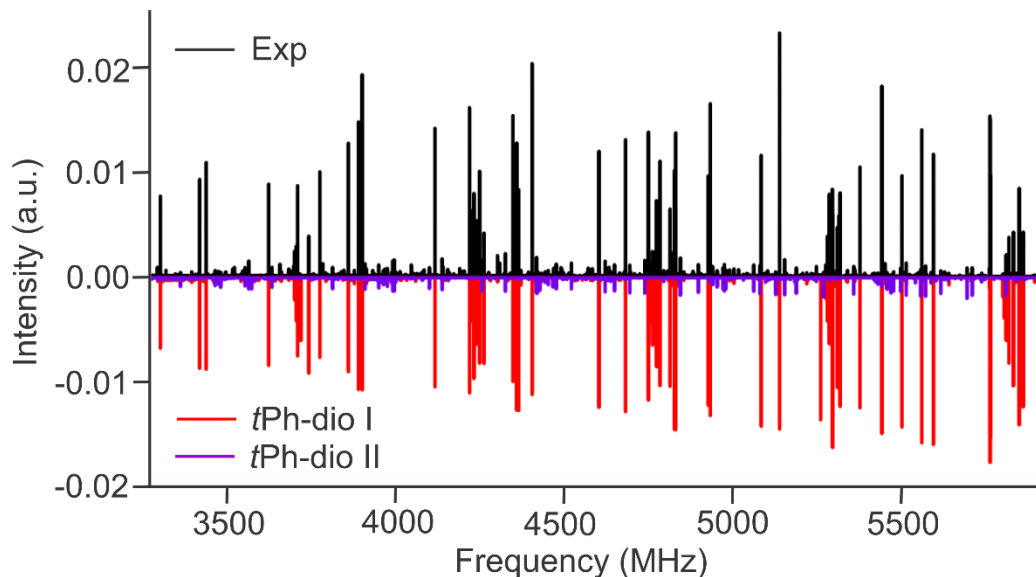


Figure 4.3. Experimental rotational spectrum recorded with a mixture of PhTFE+1,4-dioxane in helium using a 2-6 GHz CP-FTMW spectrometer. The transitions of the PhTFE monomer and PhTFE \cdots H₂O are removed for clarity. The simulated spectra were generated using the experimental spectroscopic constants, the calculated electric dipole moment components and an estimated rotational temperature of 3 K. The relative abundance of *t*Ph-dio I : *t*Ph-dio II is approximately 15 : 0.85 \approx 95% : 5%.

4.2.3 Conformational conversion

There are several low energy PhTFE \cdots 1,4-dioxane conformers, such as *t*Ph-dio III and IV, which are within an energy window of 1 kJ mol⁻¹ of the global minimum, *t*Ph-dio I. For hydrogen bonded complexes between an alcohol and an ether molecule, conformers within such a narrow energy window of 1~2 kJ mol⁻¹ have been routinely detected experimentally in rotational spectroscopic studies, for example in glycidol \cdots propylene oxide [21] and in 2-fluoroethanol \cdots propylene oxide [22]. A conformational temperature for similar hydrogen bonded systems was estimated to be 40~70 K [23]. Assuming a conformational temperature of 55 K, the percentage abundances of the first four low energy conformers are predicted to be about 57% : 21% : 14% : 8% whereas the abundances of the higher energy conformers are essentially zero. This differs significantly from the experimental abundance ratio of 95% : 5% for *t*Ph-dio I versus *t*Ph-dio II.

We therefore examined the possible conformational conversion paths among these low energy conformers. All low energy PhTFE \cdots 1,4-dioxane conformers listed in Table 4.1 feature an intermolecular O-H \cdots O hydrogen bond and the energy differences among them are mainly produced by how the other parts of the PhTFE and 1,4-dioxane subunits are orientated relative to

each other. To investigate the conversion paths between the binary conformers, we performed two different one-dimensional relaxed PES scans. One of them is along the dihedral angle (O20-O26-O9-C8) in PhTFE-1,4-dioxane, where the PhTFE and 1,4-dioxane subunits rotate against each other about the intermolecular O-H \cdots O hydrogen bond with the starting point at *t*Ph-dio II. The second one is along the dihedral angle (O20-O26-C8-C12), also corresponding to a rotation about the intermolecular O-H \cdots O hydrogen bond with the starting point at *t*Ph-dio I. The results are summarized in Figure 4.4 where several valleys and transition states can be identified. In general, the geometries obtained in the valleys in the scans are already very close to the final optimized conformational geometries and each valley is labelled with the corresponding conformer. The ZPE corrected barriers are also provided in Figure 4.4. The ZPE corrected barriers were estimated from the difference between the ZPE corrected energies of the transition states and the conformers shown in Figure 4.4.

As can be seen in Figure 4.4, the one-dimensional, relaxed PES scans are not smooth. The discontinuities happen where a low energy configuration emerges at the fixed dihedral angle value but its other dihedral angles (i.e. binding topologies) differ significantly [24]. For the same reason, even a scan of 360 degree may not return to the same starting conformer because during the scan some other dihedral angles may have altered drastically and could not return to the initial values. For example, in scan (a), the starting and ending conformers are different after a full 360 degree scan, whereas in scan (b), the same conformer is identified. In scan (a), conformers I, II, III, IV, VIII, and XII are identified along the scan path. It is clear that the energy barriers separating III from I and IV from I are very low, i.e., less than 1 kJ mol⁻¹. These low barriers can be easily overcome, based on the empirical cut-off value of 4.8 kJ mol⁻¹, below which conformational relaxation is deemed to occur substantially in a supersonic jet expansion [25]. As a result, conformers III and IV could not be detected experimentally. While II is separated from I via a high barrier of \sim 10 kJ mol⁻¹, conformational cooling can, however, still occur via a very low barrier to the slightly higher energy conformer IV and then via a second low barrier to the global minimum. This explains the relative abundance of conformer II observed is much lower than that predicted directly from the minimum energies. A much lower conformational temperature of 18 K would provide a relative abundance prediction (i.e. I : II : III : IV \sim 94% : 5% : 1% : 0%) similar to that observed for I : II experimentally. The above analysis highlights some current challenges in using abundances obtained from jet expansion experiments to benchmark theoretical relative energies.

On the other hand, the capability of rotational spectroscopy in clearly identifying individual conformers offers important experimental data to explore the conformational landscapes of these hydrogen bonded systems including their interconversion dynamics.

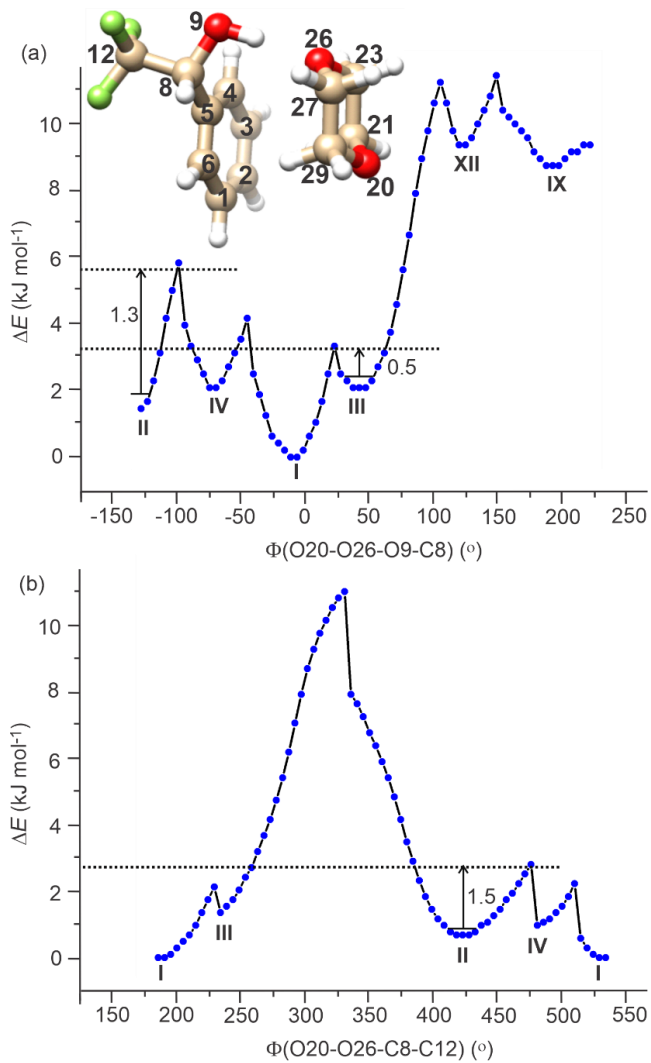


Figure 4.4. (a) One-dimensional, relaxed potential energy scan of PhTFE-1,4-dioxane starting from *t*Ph-dio II along the dihedral angle $\Phi(\text{O20-O26-O9-C8})$ at the B3LYP-D3(BJ)/def2-TZVP level of theory. (b) One-dimensional, relaxed potential energy scan of PhTFE-1,4 dioxane starting from *t*Ph-dio I along the dihedral angle $\Phi(\text{O20-O26-C8-C12})$ at the B3LYP-D3(BJ)/def2-TZVP level of theory. The energies of some relevant *ZPE* corrected barriers (in kJ mol⁻¹) are also indicated. Note that the PhTFE-1,4-dioxane conformers are indicated with their energy ordering, i.e. I, II, etc. The atom numberings are given for the C and O atoms only for clarity.

4.2.4 The role of dispersion interactions

As mentioned before, all low energy conformers listed in Table I feature an O-H \cdots H intermolecular hydrogen bond, whereas the higher energy conformers (Table S1) do not contain such an intermolecular hydrogen bond. One important question is how much do different physical interactions, such as electrostatic, induction, dispersion and exchange, contribute to the relative stability of the conformers in Table I. To quantitatively understand the nature of the non-covalent interactions in PhTFE \cdots 1,4-dioxane, SAPT analyses were performed on the eleven most stable conformers and one from the less stable group which has no O-H \cdots O hydrogen bond. The results are summarized in Table 3, along with the SAPT results of the related HFIP \cdots 1,4-dioxane [14] and H₂O \cdots 1,4-dioxane [26] complexes which were studied before using rotational spectroscopy. Note that while the SAPT analyses provide the interaction energies between the specific monomer conformers in the binary complexes, the influence of the subunit stability on the overall stability of the binary conformers is not taken into account in the SAPT analyses. For example, while *g*-Ph-dio VI and *g*-Ph-dio VII have the largest E_{total} values, they are not the most stable ones because they are made of the least stable PhTFE subunit, i.e., *g*-PhTFE.

As can be seen from Figure 4.3, the OH \cdots O interaction can occur in the axial or equatorial configurations and five out of the six most stable conformers are axial, whereas *t*Ph-V is equatorial. From the SAPT analyses of the first six conformers of PhTFE \cdots 1,4-dioxane, one can see that E_{total} is larger for the axial conformers, i.e. *t*Ph-dio I, II, III, IV, and *g*-Ph-dio VI than the equatorial one, i.e. *t*Ph-dio V, indicating that the axial OH \cdots O hydrogen bonding topology provides greater stabilization than the equatorial one.

In the previous solution NMR study of the mixed solvents of HFIP with 1,4-dioxane and PhTFE with 1,4-dioxane [4], HFIP was shown to have a stronger hydrogen bonding capability. It is interesting to note that HFIP \cdots 1,4-dioxane has the largest electrostatic and induction attractive interactions among all the binary species listed in Table 4.3, suggesting the same trend in the hydrogen bonding capability of HFIP versus PhTFE in the gas phase as in solution. In terms of dispersion interactions, conformers VI and VII of PhTFE \cdots 1,4-dioxane have the largest values, since the *g*-conformation of PhTFE enables close contact between the aromatic and the 1,4-dioxane rings. Compared with HFIP \cdots 1,4-dioxane, the addition of the phenyl group decreases the electrostatic and induction attractive interactions somewhat, but increases the dispersion

interaction significantly. Among the most stable conformers of *t*PhTFE⋯1,4-dioxane, *t*Ph-dio I is significantly stabilized by the dispersion interactions compared to *t*Ph-dio II which was also detected experimentally and *t*Ph-dio III which was not observed.

Table 4.3. The SAPT energy terms (in kJ mol⁻¹) of the eleven lowest energy PhTFE⋯1,4-dioxane conformers and two related 1,4-dioxane containing complexes, H₂O⋯1,4-dioxane [26] and HFIP⋯1,4-dioxane [14].

Complex	E_{total}	$E_{electrostatics}$	$E_{exchange}$	$E_{induction}$	$E_{dispersion}$
H ₂ O⋯1,4-dioxane	-24.9	-45.9	56.9	-16.6	-19.3
HFIP⋯1,4-dioxane	-43.5	-63.1	82.7	-30.2	-32.9
<i>t</i> Ph-dio I	-43.6	-59.9	86.2	-25.2	-44.6
<i>t</i> Ph-dio II	-43.0	-60.7	82.6	-24.6	-40.3
<i>t</i> Ph-dio III	-42.0	-58.5	81.5	-24.0	-40.9
<i>t</i> Ph-dio IV	-42.5	-58.2	83.7	-24.5	-43.4
<i>t</i> Ph-dio V	-40.5	-56.6	79.7	-22.8	-40.8
<i>g</i> -Ph-dio VI	-46.1	-63.2	91.9	-26.3	-48.5
<i>g</i> -Ph-dio VII	-44.8	-61.4	87.7	-25.4	-45.7
<i>g</i> +Ph-dio VIII	-37.4	-58.9	75.4	-24.8	-29.1
<i>g</i> -Ph-dio IX	-41.5	-62.4	81.0	-24.7	-35.4
<i>g</i> +Ph-dio X	-36.7	-54.1	71.3	-23.3	-30.6
<i>g</i> -Ph-dio XI	-42.5	-60.6	87.2	-24.7	-44.4
<i>g</i> -Ph-dio XX	-24.4	-27.0	36.2	-7.2	-26.4

Additionally, QTAIM and NCI analyses were performed to examine close intermolecular contacts in the PhTFE⋯1,4-dioxane conformers and to complement the SAPT analyses above. The QTAIM and NCI results of four representative PhTFE⋯TFE conformers are shown in Figure 4.5, including the QTAIM bond paths, bonding critical points (BCPs), and the NCI reduced density gradient isosurfaces. The results from related analyses of the three most stable PhTFE⋯TFE conformers are given in Figure S1 of Appendix B. The bond energies associated with each critical point of an intermolecular bond was estimated using a recently derived approximate equation, specifically designed for neutral hydrogen bonded systems: E_{bond} (kcal mol⁻¹) = -223.08 × ρ_{BCP} (atomic unit) + 0.7423, where ρ_{BCP} is the electron density at the bond critical point (BCP) [27]. For *t*Ph-dio I, *t*Ph-dio V and *g*-Ph-dio XI, the O-H⋯O bond energies are similar, spanning a range of 29.1 to 31.4 kJ mol⁻¹, whereas *g*-Ph-dio XX has no O-H⋯O bond. The other close intermolecular

contacts, such as the C \cdots H-C and F \cdots H-C (defined as from PhTFE to 1,4-dioxane) contacts, contribute about 2 to 4 kJ mol $^{-1}$ in the four conformers shown in Figure 4.5, whereas the C-H \cdots O contacts provide the main binding energy for *g*-Ph-dio XX. It is also interesting to note that the QTAIM analyses identified some intramolecular BCPs for the F \cdots H-C contacts inside the PhTFE subunit in *g*-Ph-dio XI and *g*-Ph-dio XX, while some attractive intramolecular interactions for the C-H \cdots O and C-H \cdots F contacts were revealed by the NCI isosurface plots in *t*Ph-dio I and in *t*Ph-dio V. The QTAIM and NCI plots of the three most stable binary conformers (see Figure S1, Appendix B) indicate that they exhibit very similar intermolecular interactions. It would be difficult to justify their minor energy differences using the QTAIM and NCI plots alone.

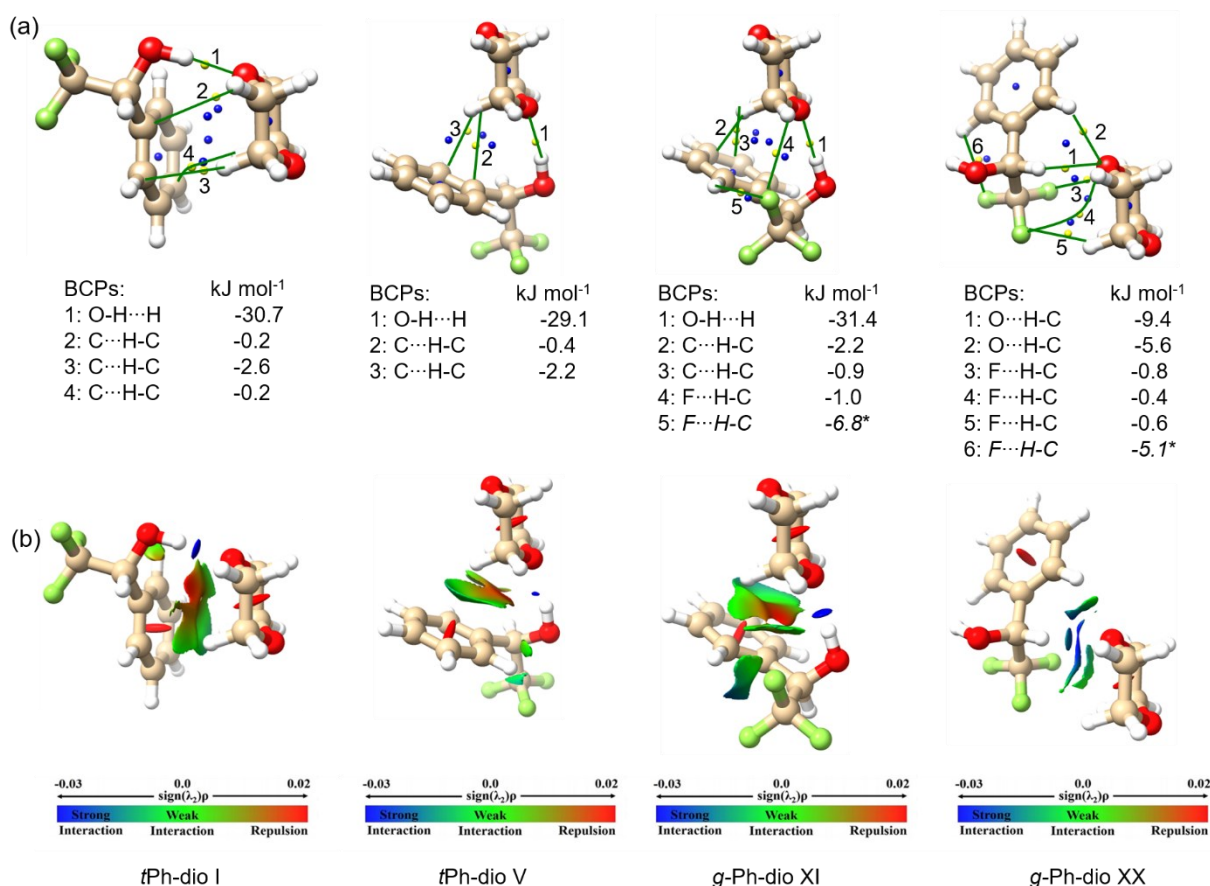


Figure 4.5. (a) The QTAIM analyses of the four representative PhTFE \cdots 1,4-dioxane conformers: *t*Ph-dio I, *t*Ph-dio II and *t*Ph-dio III. Yellow dots represent the bond critical points, orange lines represent the corresponding bond paths, and yellow dots represent ring critical points. The associated non-covalent bond energies are also listed. * emphasizes that the BCP identified corresponds to an *intramolecular* bond. See the main text for discussions. (b) The corresponding NCI isosurfaces of the four PhTFE \cdots 1,4-dioxane conformers.

4.3 Conclusion

The intermolecular interactions between PhTFE and 1,4-dioxane, two important solvents for organic reactions, were investigated using rotational spectroscopy and DFT calculations. Although 1,4-dioxane has only one relevant conformation, the phenyl group of PhTFE introduces a set of diverse geometries in the binary complex that are related to the relative orientation of the phenyl and 1,4-dioxanes rings. Rotational transitions of the two most stable conformers, *t*Ph-dio I and *t*Ph-dio II, were observed and assigned, and their experimental abundances estimated. Relaxed, one-dimensional scans along two important dihedral angles indicate that the higher energy conformers, *t*Ph-dio III and IV, can efficiently cool to *t*Ph-dio I, the global minimum, in a jet expansion because of the low conversion barriers. Interestingly, the cooling of *t*Ph-dio II to *t*Ph-dio I is greatly suppressed because *t*Ph-dio II is separated from *t*Ph-dio I by a higher energy conformer, *t*Ph-dio IV even though the related barriers are fairly low. SAPT analyses reveal that *t*Ph-dio I is substantially stabilized by dispersion interactions relative to *t*Ph-dio II. The hydrogen bonding interaction with 1,4-dioxane changes the dominant PhTFE configuration from *g*⁺ in the isolated monomeric form to *t* in the binary complex, as demonstrated experimentally and theoretically in the current study.

4.4 Experimental and computational Methods

The rotational spectrum of the PhTFE···1,4-dioxane complex was recorded using a 2-6 GHz CP-FTMW spectrometer [28,29]. The typical full width at half height of a rotational transition is ~125 kHz, and the frequency uncertainty is ~10 kHz. This spectrometer was built based on the previously reported 2-8 GHz CP-FTMW spectrometer by Pate and co-workers [30]. 1,4-dioxane (99.8% purity) and racemic PhTFE (98% purity) were purchased from Millipore-Sigma, and used without further purification. Gaseous mixtures of about 0.5% 1,4-dioxane in helium and in neon (Praxair, 99.999%) at a total pressure of ~ 3 bar and ~ 2 bar, respectively were used, while the PhTFE liquid was placed directly inside a modified General Valve nozzle cap [31] and heated to ~ 45 °C. A 12 Gs s⁻¹ arbitrary waveform generator (AWG) was used to generate a 2-6 GHz, 1 μs chirped pulse, which was amplified with a 400 W traveling wave tube (TWT) amplifier. The MW field strength used was 1/4 of the maximum possible in our set up. The amplified chirped pulse was broadcasted with a horn antenna which is situated perpendicular to the pulsed molecular beam,

and the free induction decay (FID) signal was collected by a receiving horn antenna on the opposite side. The FID signal was digitized and averaged using a 25 Gs s⁻¹ oscilloscope and Fourier transformed to give the frequency domain spectrum. For every gas pulse, six FIDs were recorded and a total of about 575k to 700k FIDs were averaged in helium and in neon, respectively. The data obtained in helium and neon are similar, and we used the data in helium for the remainder of the paper.

CREST (conformer-rotamer ensemble sampling tool), a computer code developed by Grimme and co-workers, [32] was used to generate low energy candidates for the binary PhTFE...1,4-dioxane complex. The CREST code utilized the previously developed semiempirical extended tight-binding quantum chemistry method (GFN2-xTB) [33] and can quickly explore and screen the conformational space of molecules with up to about 1000 atoms. Additionally, relaxed potential energy surface (PES) scans along dihedral angles of interest were also carried out to complement the CREST conformational searches. The structural candidates generated were subjected to subsequent geometry optimizations and harmonic frequency calculations. Specifically, the B3LYP [34,35] functional including empirical D3 dispersion corrections [36] and Becke-Johnson damping [37] was employed for all calculations together with the 6-311++G (2d,p) [38] and def2-TZVP basis sets [39,40]. Zero-point energy (ZPE) and basis set superposition error (BSSE) corrections were applied to the relative energies reported where the BSSE corrections were calculated using the counterpoise procedure [41]. All DFT calculations were completed with the Gaussian 16 suite of programs [42].

References

- [1] P. Shah, A. Westwell, *J. Enzyme Inhib. Med. Chem.* **2007**, *22*, 527-540.
- [2] T. Fujiwara, D. O'Hagan, J. Fluor, *Chem.* **2014**, *167*, 16-29.
- [3] T. Bhattacharya, A. Ghosha, D. Maiti, *Chem. Sci.*, **2021**, *12*, 3857.
- [4] A. Berkessel, J. A. Adrio, D. Hüttenhain, J. M. Neudörfl, *J. Am. Chem. Soc.* **2006**, *128*, 8421-8426.
- [5] A. Berkessel, J. A. Adrio, *Adv. Synth. Catal.* **2004**, *346*, 275-280.

-
- [6] G. G. Brown, B. C. Dian, K. O. Douglass, S. M. Geyer, S. T. Shipman and B. H. Pate, *Rev. Sci. Instrum.*, **2008**, *79*, 053103.
- [7] C. B. Park, R. W. Field, *J. Chem. Phys.* **2016**, *144*, 200901.
- [8] M. Becucci, S. Melandri, *Chem. Rev.* **2016**, *116*, 5014-5037.
- [9] X. Liu, N. Borho, Y. Xu, *Chem. Eur. J.* **2009**, *15*, 270-277.
- [10] N. A. Seifert, J. Thomas, W. Jäger, Y. Xu, *Phys. Chem. Chem. Phys.* **2018**, *20*, 27630-27637.
- [11] J. Thomas, Y. Xu, *J. Phys. Chem. Lett.* **2014**, *5*, 1850-1855.
- [12] S. Oswald, M. A. Suhm, *Angew. Chem. Int. Ed.* **2017**, *56*, 12672-12676.
- [13] S. Oswald, N. A. Seifert, F. Bohle, M. Gawrilow, S. Grimme, W. Jäger, Y. Xu, and M. A. Suhm, *Angew. Chem. Int. Ed.* **2019**, *58*, 5080-5084.
- [14] Q. Yang, F. Xie, T. Lu, N. Bui, W. Jäger, Y. Xu, *J. Mol. Spectrosc.* **2021**, *376*, 111408.
- [15] A. Shahi, E. Arunan, *J. Phys. Chem. A.* **2015**, *119*, 5650-5657.
- [16] C. D. Carlson, N. A. Seifert, M. Heger, F. Xie, J. Thomas, Y. Xu, *J. Mol. Spectrosc.* **2018**, *351*, 62-67.
- [17] L.-H. Xu, G. T. Fraser, F. J. Lovas, R. D. Suenram, C. W. Gillies, H. E. Warner, J. Z. Gillies, *J. Chem. Phys.* **1995**, *103*, 9541.
- [18] C. D. Carlson, D. Mason, Q. Yang, N. A. Seifert, Y. Xu, manuscript in preparation.
- [19] J. K. G. Watson, in: J. R. Durig (Ed.), *Vibrational Spectra and Structure*, vol. 6, Elsevier, New York, 1977, pp. 1-89.
- [20] C. M. Western, *J. Quant. Spectrosc. Radiat. Transf.* **2017**, *186*, 221-242.
- [21] J. Thomas, F. X. Sunahori, N. Borho, Y. Xu, *Chem. Eur. J.* **2011**, *17*, 4582-4587.
- [22] N. Borho, Y. Xu, *J. Am. Chem. Soc.* **2008**, *130*, 5916-5921.
- [23] N. Borho, Y. Xu, *Phys. Chem. Chem. Phys.* **2007**, *9*, 4514-4520.
- [24] T. Lu, Talking about using Gaussian for potential energy surface scanning. <http://sobereva.com/474> (accessed Feb 04, 2022).
- [25] R. S. Ruoff, T. D. Klots, T. Emilsson, H. S. Gutowsky, *J. Chem. Phys.* **1990**, *93*, 3142-3150.
- [26] Q. Gou, L. Evangelisti, G. Feng, G. Guidetti, W. Caminati, *Mol. Phys.* **2014**, *112*, 2419-2423.
- [27] S. Emamian, T. Lu, H. Kruse, H. Emamian, *J. Comput. Chem.* **2019**, *40*, 2868-2881.
- [28] F. Xie, X. Ng, N. A. Seifert, J. Thomas, W. Jäger, Y. Xu, Rotational spectroscopy of chiral tetrahydro-2-furoic acid: Conformational landscape, conversion, and abundances. *J. Chem. Phys.* **2018**, *149*, 224306.

-
- [29] F. Xie, N. A. Seifert, M. Heger, J. Thomas, W. Jäger, Y. Xu, *Phys. Chem. Chem. Phys.* **2019**, *21*, 15408-15416.
- [30] C. Pérez, S. Lobsiger, N. A. Seifert, D. P. Zaleski, B. Temelso, G. C. Shields, Z. Kisiel and B. H. Pate, *Chem. Phys. Lett.* **2013**, 1-15.
- [31] F. Xie, N. A. Seifert, W. Jäger, Y. Xu, *Angew. Chem. Int. Ed.* **2020**, *59*, 15703-15710.
- [32] P. Pracht, F. Bohle, S. Grimme, *Phys. Chem. Chem. Phys.* **2020**, *22*, 7169-7192.
- [33] S. Grimme, C. Bannwarth, P. Shushkov, *J. Chem. Theory Comput.* **2017**, *13*, 1989-2009.
- [34] A. D. Becke, *J. Chem. Phys.* **1993**, *98*, 5648-5652.
- [35] P. J. Stephens, F. J. Devlin, C. F. Chabalowski, M. J. Frisch, *J. Phys. Chem.* **1994**, *98*, 11623-11627.
- [36] S. Grimme, S. Ehrlichm, L. Goerigk, *J. Comp. Chem.* **2011**, *32*, 1456-1465.
- [37] A. D. Becke, E. R. Johnson, *J. Chem. Phys.* **2005**, *123*, 154101.
- [38] R. Krishnan, J. S. Binkley, R. Seeger, J. A. Pople, *J. Chem. Phys.* **1980**, *72*, 650-654.
- [39] F. Weigend, R. Ahlrichs, *Phys. Chem. Chem. Phys.* **2005**, *7*, 3297-3305.
- [40] A. Schäfer, C. Huber, R. Ahlrichs, *J. Chem. Phys.* **1994**, *100*, 5829-5835.
- [41] S. F. Boys, F. Bernardi, *Mol. Phys.* **1970**, *19*, 553-566.
- [42] Gaussian 16, Revision B.01, M. J. Frisch, G. W. Trucks, H. B. Schlegel, G. E. Scuseria, M. A. Robb, J. R. Cheeseman, G. Scalmani, V. Barone, G.A. Petersson, H. Nakatsuji, X. Li, M. Caricato, A. V. Marenich, J. Bloino, B. G. Janesko, R. Gomperts, B. Mennucci, H. P. Hratchian, J. V. Ortiz, A. F. Izmaylov, J. L. Sonnenberg, D. Williams-Young, F. Ding, F. Lipparini, F. Egidi, J. Goings, B. Peng, A. Petrone, T. Henderson, D. Ranasinghe, V. G. Zakrzewski, J. Gao, N. Rega, G. Zheng, W. Liang, M. Hada, M. Ehara, K. Toyota, R. Fukuda, J. Hasegawa, M. Ishida, T. Nakajima, Y. Honda, O. Kitao, H. Nakai, T. Vreven, K. Throssell, J. A. Montgomery Jr., J. E. Peralta, F. Ogliaro, M. J. Bearpark, J. J. Heyd, E. N. Brothers, K. N. Kudin, V. N. Staroverov, T. A. Keith, R. Kobayashi, J. Normand, K. Raghavachari, A. P. Rendell, J. C. Burant, S. S. Iyengar, J. Tomasi, M. Cossi, J. M. Millam, M. Klene, C. Adamo, R. Cammi, J. W. Ochterski, R. L. Martin, K. Morokuma, O. Farkas, J. B. Foresman, D. J. Fox, Gaussian 16, Revision A.03, Gaussian, Inc., Wallingford, CT, **2016**.

Chapter 5

Conclusions and Future Work

In this thesis, I applied chirped pulse Fourier transform microwave (CP-FTMW) spectroscopy to probe structural and energetic relationships of different conformers of two fluoroalcohol...1,4 dioxane complexes, including HFIP...1,4 dioxane and PhTFE...1,4 dioxane. These studies provide a better understanding of the non-covalent interactions between these two types of important common organic solvents and how different substituents on the fluoroalcohols influence the structural-energetic properties of these complexes. The important results are summarized as follows.

In Chapter 3, the rotational spectrum of the binary complex formed between HFIP and 1,4-dioxane was investigated using a CP-FTMW spectrometer. HFIP is known to be an exceptional solvent that catalyzes the epoxidation of olefins by hydrogen peroxide. The addition of 1,4-dioxane can severely reduce HFIP's ability to boost the epoxidation rate, possibly through its intermolecular interactions with HFIP. It is therefore of considerable interest to examine the non-covalent interactions between HFIP and 1,4-dioxane in detail. Theoretical conformational searches were carried out for the binary HFIP...1,4-dioxane complex and 17 minimum energy structures were identified. Seven of them are within an energy window of 7 kJ mol^{-1} , while the three lowest energy ones are within 1.4 kJ mol^{-1} . Experimentally, only the rotational spectrum of the most stable conformer was detected and assigned. To understand the non-observation of the other low energy conformers in the supersonic jet expansion, subsequent analyses were performed to estimate the conformational conversion barriers. The detected conformer contains a *trans* HFIP subunit which is hydrogen-bonded to an O atom of 1,4-dioxane and is further stabilized by weak $\text{F}\cdots\text{H}$ attractive interactions. The intermolecular interactions in HFIP...1,4-dioxane were analyzed and visualized using QTAIM, NCI and SAPT approaches, and the interaction energies compared to the HFIP dimer and related complexes of HFIP and 1,4-dioxane with water.

In Chapter 4, a rotational spectrum of the hydrogen-bonded complex between 1-phenyl-2,2,2-trifluoroethanol (PhTFE), a chiral fluoroalcohol, and 1,4-dioxane, a common solvent for organic reactions, was measured using a chirped pulse Fourier transform microwave spectrometer. Initial theoretical conformational searches were carried out using CREST, a recently developed

conformational searching tool. Subsequent geometry optimization and harmonic frequency calculations at the B3LYP-D3(BJ)/def2-TZVP level of theory yielded nearly 30 binary conformers of which 13 are within an energy window of $\sim 5 \text{ kJ mol}^{-1}$. Interestingly, while the OH \cdots O hydrogen bond dominates the attractive binary interactions, the complex conformational landscape is mainly controlled by subtle dispersion interactions between the phenyl and 1,4-dioxane rings. Two sets of rotational transitions were assigned in the experimental spectrum and attributed to the two most stable conformers of PhTFE \cdots 1,4-dioxane. To appreciate how the phenyl ring and OH functional groups influence the intermolecular interaction and conformational distribution of the binary complex, QTAIM, NCI and SAPT analyses were employed. The main PhTFE conformation within the complex, identified experimentally, is different from that of the isolated PhTFE monomer reported previously, but the same as that observed in a solvent mixture of PhTFE and 1,4-dioxane in the condensed phase.

The two projects in this thesis contribute to our understanding of the properties of fluoroalcohols as co-solvents, such as the "booster effect" mentioned in the introduction. The addition of 1,4-dioxane can disrupt fluoroalcohol multimer interactions, resulting in a decrease in the reaction rate. They provide insights into how non-covalent interactions influence the properties of the mixed solvents containing fluoroalcohols and allow one to examine how the OH orientation and other conformational preferences of an isolated fluoroalcohol molecule are modified by the hydrogen-bonding interactions in the corresponding aggregates.

It would be very interesting to extend the study to ternary and larger molecular systems beyond the two binding partners. For example, larger aggregates would provide opportunities to examine how the preferred binding topologies change with the addition of a further fluoroalcohol molecule. With the high sensitivity achieved with the two existing microwave spectrometers in our laboratory, I think such a study is feasible. In terms of theoretical modelling, one can expect that these larger molecular systems would have many more possible conformations and the challenge to identify all possible low energy geometries would be considerable, as would the spectroscopic assignment.

Bibliography

- [1] P. Shah, A. Westwell, *J. Enzyme Inhib. Med. Chem.* **2007**, *22*, 527-540.
- [2] C. Isanbor, D. O'Hagan, *J. Fluor. Chem.* **2006**, *127*, 303-319.
- [3] Berkessel, J. A. Adrio, D. Hggtenhain, J. M. Neudörfl, *J. Am. Chem. Soc.* **2006**, *128*, 8421-8426.
- [4] X. Liu, N. Borho and Y. Xu, *Eur. J. Chem.* **2009**, *15*, 270-277.
- [5] J. Thomas and Y. Xu, *J. Phys. Chem. Lett.* **2014**, *5*, 1850-1855.
- [6] J. Thomas, N. A. Seifert, W. Jäger and Y. Xu, *Angew. Chem. Int. Ed.* **2017**, *56*, 6289-6293.
- [7] J. Thomas, X. Liu, W. Jäger and Y. Xu, *Angew. Chem. Int. Ed.* **2015**, *54*, 11711-11715.
- [8] N. A. Seifert, J. Thomas, W. Jäger, and Y. Xu, *Phys. Chem. Chem. Phys.* **2018**, *20*, 27630-27637.
- [9] Berkessel, J. A. Adrio, *Adv. Synth. Catal.* **2004**, *346*, 275-280.
- [10] G. B. Park and R. W. Field, *J. Chem. Phys.*, **2016**, *144*, 200901.
- [11] G. G. Brown, B. C. Dian, K. O. Douglass, S. M. Geyer, S. T. Shipman and B. H. Pate, *Rev. Sci. Instrum.*, **2008**, *79*, 053103.
- [12] D. Carlson, N. A. Seifert, M. Heger, F. Xie, J. Thomas, Y. Xu, *J. Mol. Spectrosc.* **2018**, *351*, 62-67.
- [13] F. Xie, X. Ng, N. A. Seifert, J. Thomas, W. Jäger, Y. Xu, *J. Chem. Phys.* **2018**, *149*, 224306.
- [14] F. Xie, N. A. Seifert, M. Heger, J. Thomas, W. Jäger, Y. Xu, *Phys. Chem. Chem. Phys.* **2019**, *21*, 15408-15416.
- [15] M. Becucci, S. Melandri, *Chem. Rev.* **2016**, *116*, 5014-5037.
- [16] D.-P. Hong, M. Hoshino, R. Kuboi, Y. Goto, *J. Am. Chem. Soc.* **1999**, *121*, 8427-8433.
- [17] J. M. Brown, J. M. Brown, A. Carrington, *Rotational spectroscopy of diatomic molecules*, Cambridge University Press, **2003**.
- [18] W. Gordy, R. L. Cook, *Microwave molecular spectra*, Wiley, **1984**.
- [19] H. Townes, A. L. Schawlow, *Microwave spectroscopy*, Courier Corporation, **2013**.
- [20] P. F. Bernath, *Spectra of Atoms and Molecules*, New York, **1995**.
- [21] J. C. Mcgurk, W. H. Flygare, *J. Chem. Phys.*, **1973**, *59*, 5742-5743.

- [22] T. G. Schmalz, W. H. Flygare, *Laser and Coherence Spectroscopy* (Ed.; J. I. Steinfeld), Plenum, New York, **1978**, pp. 125-196.
- [23] L. Allen, J. H. Eberly, *Optical resonance and two-level atoms*, Courier Corporation, **2012**.
- [24] C. Pérez, S. Lobsiger, N. A. Seifert, D. P. Zaleski, B. Temelso, G. C. Shields, Z. Kisiel, B. H. Pate, *Chem. Phys. Lett.* **2013**, 1-15.
- [25] J. U. Grabow, W. Stahl, *Z Naturforsch.* **1990**, *45A*, 1043-1044.
- [26] J. U. Grabow, W. Stahl, H. Dreizler, *Rev. Sci. Instrum.*, **1996**, *67*, 4072-4084.
- [27] E. Arunan, S. Dev, P. K. Mandal, *Appl. Spectrosc. Rev.*, **2004**, *39*, 131-181.
- [28] S. Grimme, *J. Chem. Theory Comput.* **2019**, *15*, 2847-2862.
- [29] S. Grimme, C. Bannwarth, and P. Shushkov, *J. Chem. Theory Comput.* **2017**, *13*, 1989-2009.
- [30] S. Grimme, C. Bannwarth, S. Dohm, A. Hansen, J. Pisarek, P. Pracht, J. Seibert, and F. Neese, *Angew Chem. Int. Ed.* **2017**, *56*, 14763-14769; *Angew. Chem.* **2017**, *129*, 14958-14964.
- [31] Xie, M. Fusè, A. S. Hazrah, W. Jäger, V. Barone, Y. Xu, *Angew. Chem. Int. Ed.*, **2020**, *59*, 22427-22430.
- [32] T. Lu, F. Xie, N. A. Seifert, W. Jäger, Y. Xu, *J. Mol. Struct.* **2020**, *1217*, 128359.
- [33] *in Ideas of Quantum Chemistry* (Ed.: L. Piela), Elsevier, Amsterdam, **2007**, pp. 567-614.
- [34] J. C. Slater, *Phys. Rev.*, **1952**, *87*, 807-835.
- [35] Moller, M. S. Plesset, *Phys. Rev.*, **1934**, *46*, 0618-0622.
- [36] S. Grimme, J. Antony, S. Ehrlich, H. Krieg, *J. Chem. Phys.*, **2010**, *132*, 154104.
- [37] S. Grimme, R. Huenerbein, S. Ehrlich, *ChemPhysChem*, **2011**, *12*, 1258-1261.
- [38] S. Grimme, S. Ehrlich, L. Goerigk, *J. Comput. Chem.*, **2011**, *32*, 1456-1465.
- [39] F. Weigend, R. Ahlrichs, *Phys. Chem. Chem. Phys.* **2005**, *7*, 3297-3305.
- [40] Schäfer, C. Huber, R. Ahlrichs, *J. Chem. Phys.* **1994**, *100*, 5829-5835.
- [41] M. Western, *J. Quant. Spectrosc. Radiat. Transf.*, **2017**, *186*, 221-242.
- [42] R. F. W. Bader, *Chem. Rev.* **1991**, *91*, 893-928.
- [43] R. Johnson, S. Keinan, P. Mori-Sánchez, J. Contreras-García, A. J. Cohen, W. Yang, *J. Am. Chem. Soc.* **2010**, *132*, 6498-6506.

- [44] T. Lu, F. Chen, *J. Comp. Chem.* **2012**, *33*, 580-592.
- [45] W. Humphrey, A. Dalke, K. Schulten, *J. Mol. Graph.* **1996**, *14*, 33-38.
- [46] T. M. Parker, L. A. Burns, R. M. Parrish, A. G. Ryno, C. D. Sherrill, *J. Chem. Phys.* **2014**, *140*, 094106/1-16.
- [47] R. M. Parrish, L. A. Burns, D. G. A. Smith, A. C. Simmonett, A. E. DePrince, III, E. G. Hohenstein, U. Bozkaya, A. Y. Sokolov, R. D. Remigio, R. M. Richard, J. F. Gonthier, A. M. James, H. R. McAlexander, A. Kumar, M. Saitow, X. Wang, B. P. Pritchard, P. Verma, H. F. Schaefer, III, K. Patkowski, R. A. King, E. F. Valeev, F. A. Evangelista, J. M. Turney, T. D. Crawford, C. D. Sherrill, *J. Chem. Theory Comput.* **2017**, *13*, 3185-3197.
- [48] Isanbor, D. O'Hagan, *J. Fluor. Chem.* **2006**, *127*, 303-319.
- [49] J. C. Biffinger, H. W. Kim, S. G. DiMagno, *ChemBioChem* **2004**, *5*, 622-627.
- [50] Thomas and Y. Xu, *J. Phys. Chem. Lett.* **2014**, *5*, 1850-1855.
- [51] Shahi, E. Arunan, *J. Phys. Chem. A* **2015**, *119*, 5650-5657.
- [52] S. Oswald, M. A. Suhm, *Angew. Chem. Int. Ed.* **2017**, *56*, 12672-12676.
- [53] S. Oswald, N. A. Seifert, F. Bohle, M. Gawrilow, S. Grimme, W. Jäger, Y. Xu, and M. A. Suhm, *Angew. Chem. Int. Ed.* **2019**, *58*, 5080-5084
- [54] Wu, N. A. Seifert, S. Oswald, W. Jäger, Y. Xu, to be submitted.
- [55] Wu, N. A. Seifert, S. Oswald, Y. Xu, to be submitted.
- [56] J. K. G. Watson, in: J. R. Durig (Ed.), *Vibrational Spectra and Structure*, vol. 6, Elsevier, New York, 1977, pp. 1-89.
- [57] Espinosa, E. Molins, C. Lecomte, *Chem. Phys. Lett.* **1998**, *285*, 170-173.
- [58] Mata, I. Alkorta, E. Espinosa, E. Molins, *Chem. Phys. Lett.* **2011**, *507*, 185-189.
- [59] R. S. Ruoff, T. D. Klots, T. Emilsson, H. S. Gutowsky, *J. Chem. Phys.* **1990**, *93*, 3142-3150.
- [60] J. T. A. Gall, J. Thomas, F. Xie, Z. Wang, W. Jäger, Y. Xu, *Phys. Chem. Chem. Phys.* **2017**, *19*, 29508-29515.
- [61] W. Huang, J. Thomas, W. Jäger, Y. Xu, *Phys. Chem. Chem. Phys.* **2017**, *19*, 12221-12228.
- [62] F. Xie, N. A. Seifert, W. Jäger, Y. Xu, *Angew. Chem. Int. Ed.* **2020**, *59*, 15703-15710.

- [63] Gaussian 16, Revision B.01, M. J. Frisch, G. W. Trucks, H. B. Schlegel, G. E. Scuseria, M. A. Robb, J. R. Cheeseman, G. Scalmani, V. Barone, G.A. Petersson, H. Nakatsuji, X. Li, M. Caricato, A. V. Marenich, J. Bloino, B. G. Janesko, R. Gomperts, B. Mennucci, H. P. Hratchian, J. V. Ortiz, A. F. Izmaylov, J. L. Sonnenberg, D. Williams-Young, F. Ding, F. Lipparini, F. Egidi, J. Goings, B. Peng, A. Petrone, T. Henderson, D. Ranasinghe, V. G. Zakrzewski, J. Gao, N. Rega, G. Zheng, W. Liang, M. Hada, M. Ehara, K. Toyota, R. Fukuda, J. Hasegawa, M. Ishida, T. Nakajima, Y. Honda, O. Kitao, H. Nakai, T. Vreven, K. Throssell, J. A. Montgomery Jr., J. E. Peralta, F. Ogliaro, M. J. Bearpark, J. J. Heyd, E. N. Brothers, K. N. Kudin, V. N. Staroverov, T. A. Keith, R. Kobayashi, J. Normand, K. Raghavachari, A. P. Rendell, J. C. Burant, S. S. Iyengar, J. Tomasi, M. Cossi, J. M. Millam, M. Klene, C. Adamo, Cammi, J. W. Ochterski, R. L. Martin, K. Morokuma, O. Farkas, J. B. Foresman, D. J. Fox, Gaussian 16, Revision A.03, Gaussian, Inc., Wallingford, CT, 2016
- [64] D. Becke, *J. Chem. Phys.* **1993**, *98*, 5648-5652.
- [65] P. J. Stephens, F. J. Devlin, C. F. Chabalowski, M. J. Frisch, *J. Phys. Chem.* **1994**, *98*, 11623-11627.
- [66] Stefan, E. Stephan, G. Lars, *J. Comp. Chem.* **2011**, *32*, 1456-1465.
- [67] D. Becke, E. R. Johnson, *J. Chem. Phys.* **2005**, *123*, 154101.
- [68] S. F. Boys, F. Bernardi, *Mol. Phys.* **1970**, *19* (4), 553-566.
- [69] Peng, H. B. Schlegel, *Isr. J. Chem.* **1993**, *33*, 449-454.
- [70] L.H. Xu, G.T. Fraser, F.J. Lovas, R.D. Suenram, C.W. Gillies, H.E. Warner, J.Z. Gillies, *J. Chem. Phys.* **1995**, *103*, 9541-9548.
- [71] S. Emamian, T. Lu , H. Kruse , H. Emamian, *J. Comput. Chem.* **2019**, *40*, 2868-2881.
- [72] Q. Gou, L. Evangelisti, G. Feng, G. Guidetti. W. Caminati, *Mol. Phys.* **2014**, *112*, 2419-2423.
- [73] N. Borho, Y. Xu, *Phys. Chem. Chem. Phys.* **2007**, *9*, 4514-4520.
- [74] N. Borho, Y. Xu, *J. Am. Chem. Soc.* **2008**, *130*, 5916-5921.
- [75] J. Thomas, F. X. Sunahori, N. Borho, Y. Xu, *Chem. Eur. J.* **2011**, *17*, 4582-4587.
- [76] C. M. Western, *J. Quant. Spectrosc. Radiat. Transf.* **2017**, *186*, 221-242.
- [77] A. D. Becke, *J. Chem. Phys.* **1993**, *98*, 5648-5652.

- [78] L.-H. Xu, G. T. Fraser, F. J. Lovas, R. D. Suenram, C. W. Gillies, H. E. Warner, J. Z. Gillies, *J. Chem. Phys.* **1995**, *103*, 9541.
- [79] T. Fujiwara, D. O'Hagan, J. Fluor, *Chem.* **2014**, *167*, 16-29.
- [80] T. Bhattacharya, A. Ghosha, D. Maiti, *Chem. Sci.*, **2021**, *12*, 3857.

Appendix A

Supporting Information for Chapter 3

Hydrogen Bonding Interactions in the 1,1,1,3,3,3-Hexafluoro-2-Propanol...1,4-Dioxane Complex: Rotational Spectroscopy and Ab Initio Calculations

Contents:

1. Table S1-S2: Spectroscopic parameters of the ten conformers of HFIP...1,4-dioxane calculated at the B3LYP-D3(BJ)/def2-TZVP level of theory B3LYP-D3(BJ)/6-311++G(2d,p) and the MP2/6-311++G(2d,p) levels of theory
2. Tables S3-S9: DFT coordinates of the ten HFIP...1,4-dioxane in their respective principal inertial axis systems at the B3LYP-D3(BJ)/def2-TZVP level
3. Tables S10: Experimental transition frequencies of HFIP-1,4 dioxane

Table S1. The relative raw, *ZPE/BSSE* corrected relative energies and *ZPE/BSSE* corrected binding energies and spectroscopic parameters of the group b) conformers of the HFIP···1,4-dioxane complex calculated at the B3LYP-D3(BJ)/def2-TZVP level of theory.^a

Conformer	ΔE	ΔE_0	$\Delta E_{0(BSSE)}$	ΔE_b	<i>A</i>	<i>B</i>	<i>C</i>	μ_a	μ_b	μ_c
VIII	17.8	16.5	15.9	22.1	730	336	284	0.9	0.0	0.4
IX	19.2	17.6	17.0	21.1	751	347	297	0.4	0.1	0.5
X	20.9	19.1	19.8	19.8	810	295	256	0.6	0.1	0.5
XI	23.4	20.8	20.2	22.5	717	353	302	2.3	1.0	2.0
XII	26.1	23.3	22.5	20.2	799	296	256	2.0	1.0	2.0

^a ΔE , ΔE_0 , $\Delta E_{0(BSSE)}$ are the relative raw, *ZPE* corrected relative, and both *ZPE* and *BSSE* corrected relative energies in kJ mol^{-1} , respectively. ΔE_b is the both *ZPE* and *BSSE* corrected binding energy in kJ mol^{-1} . *A*, *B*, and *C* are the rotational constants in MHz and μ_g ($g = a, b, c$) are the electric dipole moment components in Debye.

Table S2. The relative raw, *ZPE/BSSE* corrected relative energies and *ZPE/BSSE* corrected binding energies and spectroscopic parameters of the group c) conformers of the HFIP···1,4-dioxane complex calculated at the B3LYP-D3(BJ)/def2-TZVP level of theory.^a

Conformer	ΔE	ΔE_0	$\Delta E_{0(BSSE)}$	ΔE_b	<i>A</i>	<i>B</i>	<i>C</i>	μ_a	μ_b	μ_c
XIII	34.3	32.0	31.3	6.8	777	346	284	0.5	0.0	0.3
XIV	35.6	33.0	32.0	6.1	830	299	247	0.4	0.0	0.4
XV	38.1	35.2	33.1	5.0	799	264	225	0.8	0.1	0.4
XVI	39.5	36.3	34.2	3.8	1205	184	180	0.4	0.5	0.1
XVII	44.6	40.6	38.4	4.2	1204	187	176	2.2	1.3	1.1

^a ΔE , ΔE_0 , $\Delta E_{0(BSSE)}$ are the relative raw, *ZPE* corrected relative, and both *ZPE* and *BSSE* corrected relative energies in kJ mol^{-1} , respectively. ΔE_b is the both *ZPE* and *BSSE* corrected binding energy in kJ mol^{-1} . *A*, *B*, and *C* are the rotational constants in MHz and μ_g ($g = a, b, c$) are the electric dipole moment components in Debye.

Table S3. DFT coordinates of conformer **I** of the HFIP···1,4-dioxane complex in its principal inertial axis system at the B3LYP-D3(BJ)/def2-TZVP level of theory.

Atom	<i>a</i> (Å)	<i>b</i> (Å)	<i>c</i> (Å)
O	1.858997	0.006521	1.043855
O	3.837511	0.000416	-0.952502
C	2.606033	-1.178921	0.758151
H	1.942159	-2.020339	0.953294
H	3.464927	-1.231697	1.437097
C	3.077767	-1.170473	-0.683064
H	2.213990	-1.220239	-1.357327
H	3.728669	-2.023184	-0.877694
C	2.597225	1.193500	0.742105
H	3.455763	1.261768	1.420117
H	1.927172	2.032547	0.925892
C	3.068829	1.169001	-0.698965
H	3.713126	2.023947	-0.905408
H	2.204533	1.202863	-1.373580
C	-1.591421	1.286114	-0.100423
C	-1.669735	-0.002862	0.739705
H	-2.665136	-0.005883	1.190123
C	-1.584377	-1.289991	-0.102536
F	-0.401126	1.415908	-0.720538
F	-2.548763	1.344250	-1.038277
F	-1.741338	2.351206	0.701091
F	-2.538930	-1.349996	-1.043155
F	-1.732566	-2.357132	0.696625
F	-0.391945	-1.414190	-0.719540
O	-0.736052	-0.001274	1.761600
H	0.186792	0.002127	1.416553

Table S4. DFT coordinates of conformer **II** of the HFIP···1,4-dioxane complex in its principal inertial axis system at the B3LYP-D3(BJ)/def2-TZVP level of theory.

Atom	<i>a</i> (Å)	<i>b</i> (Å)	<i>c</i> (Å)
O	-4.072044	0.539976	-0.279947
O	-1.822616	-1.131874	-0.010143
C	-3.647955	0.094823	1.000674
H	-4.542275	0.000573	1.617160
H	-2.980177	0.838673	1.455499
C	-2.930390	-1.236494	0.890814
H	-3.615872	-2.008110	0.522947
H	-2.521342	-1.548809	1.851503
C	-2.964788	0.666229	-1.163376
H	-2.277541	1.437187	-0.793964
H	-3.362972	0.982107	-2.127887
C	-2.232751	-0.655378	-1.296532
H	-1.327757	-0.551734	-1.892479
H	-2.885617	-1.404847	-1.757792
C	2.060622	-1.024894	-0.083068
C	1.471477	0.051815	0.847625
H	2.220296	0.227061	1.623368
C	1.257071	1.409570	0.151639
F	2.316439	-2.135092	0.623161
F	1.203766	-1.359194	-1.066968
F	3.209288	-0.632019	-0.655624
F	0.376852	1.322089	-0.867769
F	2.397160	1.919253	-0.336752
F	0.760866	2.291332	1.031626
O	0.310447	-0.390595	1.458690
H	-0.384192	-0.623273	0.798663

Table S5. DFT coordinates of conformer **III** of the HFIP···1,4-dioxane complex in its principal inertial axis system at the B3LYP-D3(BJ)/def2-TZVP level of theory.

Atom	<i>a</i> (Å)	<i>b</i> (Å)	<i>c</i> (Å)
O	-1.799318	-0.148371	-0.805102
O	-4.303551	0.063522	0.462314
C	-2.651877	-1.291003	-0.666696
H	-1.996599	-2.156596	-0.572920
H	-3.256549	-1.393609	-1.574368
C	-3.546354	-1.136303	0.548514
H	-2.935202	-1.129975	1.460721
H	-4.259913	-1.958412	0.608189
C	-2.556307	1.066169	-0.871651
H	-3.157442	1.058371	-1.787387
H	-1.832718	1.878833	-0.924670
C	-3.451285	1.195382	0.345867
H	-4.095800	2.070322	0.258579
H	-2.835911	1.296576	1.249566
C	1.801388	-1.258248	0.053166
C	1.355554	-0.000448	0.822442
H	1.952119	0.023876	1.736987
C	1.654115	1.316340	0.081416
F	1.576181	-2.344090	0.811647
F	1.115870	-1.417719	-1.091990
F	3.109314	-1.237578	-0.246062
F	1.311213	2.353285	0.863941
F	0.947347	1.423920	-1.058801
F	2.953105	1.450877	-0.223585
O	0.017798	-0.079566	1.177578
H	-0.564737	-0.103884	0.380330

Table S6. DFT coordinates of conformer **IV** of the HFIP···1,4-dioxane complex in its principal inertial axis system at the B3LYP-D3(BJ)/def2-TZVP level of theory.

Atom	<i>a</i> (Å)	<i>b</i> (Å)	<i>c</i> (Å)
O	4.482304	-0.097262	0.705684
O	2.219821	-0.196680	-0.967850
C	3.595496	1.010146	0.618396
H	4.194064	1.909261	0.765193
H	2.842122	0.952329	1.415084
C	2.910286	1.039866	-0.733640
H	3.645963	1.187980	-1.531305
H	2.159979	1.827358	-0.782386
C	3.790336	-1.319789	0.494996
H	3.045999	-1.472152	1.287954
H	4.530526	-2.118254	0.550223
C	3.105722	-1.319385	-0.858494
H	2.494982	-2.211488	-0.995395
H	3.848122	-1.262795	-1.661729
C	-2.246681	-1.120079	0.008201
C	-1.100727	-0.139361	-0.280262
H	-0.901301	-0.211231	-1.354714
C	-1.468346	1.332767	-0.015553
F	-1.880594	-2.353847	-0.381085
F	-2.559491	-1.175890	1.306517
F	-3.359115	-0.795103	-0.674294
F	-1.847489	1.558784	1.245348
F	-2.443692	1.764602	-0.831167
F	-0.379920	2.098903	-0.256769
O	-0.012372	-0.510147	0.498643
H	0.811614	-0.385510	-0.022627

Table S7. DFT coordinates of conformer **V** of the HFIP···1,4-dioxane complex in its principal inertial axis system at the B3LYP-D3(BJ)/def2-TZVP level of theory.

Atom	<i>a</i> (Å)	<i>b</i> (Å)	<i>c</i> (Å)
O	3.893338	-0.125962	-1.129705
O	2.248889	-0.304431	1.143344
C	3.167251	-1.313769	-0.854112
H	3.762439	-2.146054	-1.230138
H	2.208055	-1.299592	-1.390998
C	2.922568	-1.460177	0.635448
H	3.874174	-1.579666	1.164931
H	2.282416	-2.315061	0.852499
C	3.207490	1.018867	-0.640146
H	2.250442	1.136431	-1.165480
H	3.834132	1.882833	-0.861155
C	2.964978	0.901308	0.851583
H	2.353584	1.723270	1.220382
H	3.918168	0.886637	1.391265
C	-2.065584	-1.089347	-0.159389
C	-0.889966	-0.139028	0.110676
H	-0.140350	-0.361964	-0.656380
C	-1.242161	1.349370	-0.071287
F	-2.595848	-0.886156	-1.378946
F	-1.621954	-2.358893	-0.120428
F	-3.042853	-0.967466	0.742632
F	-0.148594	2.089082	0.223668
F	-2.232263	1.755598	0.726091
F	-1.579137	1.635736	-1.340374
O	-0.433198	-0.374583	1.399062
H	0.546226	-0.327289	1.398078

Table S8. DFT coordinates of conformer **VI** of the HFIP···1,4-dioxane complex in its principal inertial axis system at the B3LYP-D3(BJ)/def2-TZVP level of theory.

Atom	<i>a</i> (Å)	<i>b</i> (Å)	<i>c</i> (Å)
O	2.142852	0.249924	-0.398281
O	4.833152	0.082462	0.387806
C	2.993232	1.400809	-0.455469
H	2.359682	2.266943	-0.265698
H	3.423979	1.482542	-1.459857
C	4.094494	1.280074	0.579672
H	3.658777	1.294749	1.587836
H	4.799491	2.106542	0.488766
C	2.883706	-0.963058	-0.584696
H	3.309977	-0.972771	-1.594179
H	2.170979	-1.780343	-0.486499
C	3.985599	-1.056382	0.451728
H	4.612338	-1.929131	0.268327
H	3.545467	-1.140241	1.454415
C	-2.277709	1.119356	0.144676
C	-1.095109	0.147664	0.022747
H	-0.471327	0.313608	0.907234
C	-1.506706	-1.335560	0.069939
F	-3.101685	1.060942	-0.905667
F	-3.000589	0.882933	1.254372
F	-1.807864	2.376836	0.231119
F	-2.359812	-1.673578	-0.900435
F	-2.058732	-1.668939	1.248815
F	-0.398175	-2.095929	-0.077850
O	-0.430294	0.424424	-1.164792
H	0.533785	0.357677	-0.999811

Table S9. DFT coordinates of conformer **VII** of the HFIP···1,4-dioxane complex in its principal inertial axis system at the B3LYP-D3(BJ)/def2-TZVP level of theory.

Atom	<i>a</i> (Å)	<i>b</i> (Å)	<i>c</i> (Å)
O	2.184481	0.734896	0.286340
O	4.779725	-0.155290	-0.329666
C	2.618572	0.626095	-1.073548
H	2.105314	1.411324	-1.629238
H	2.325546	-0.352550	-1.470551
C	4.123429	0.796555	-1.153283
H	4.396934	1.813972	-0.843159
H	4.474399	0.631741	-2.172182
C	2.850198	-0.222946	1.122066
H	2.564784	-1.232884	0.810210
H	2.494987	-0.047933	2.137056
C	4.351034	-0.040907	1.020693
H	4.869864	-0.816005	1.584776
H	4.635099	0.941132	1.421578
C	-1.182120	-1.260539	-0.129475
C	-1.203710	0.280579	-0.143941
H	-0.832462	0.574212	-1.132842
C	-2.616672	0.872879	-0.033208
F	-1.726043	-1.783233	0.972121
F	-1.805712	-1.784703	-1.196945
F	0.106425	-1.672827	-0.182202
F	-3.429822	0.382402	-0.986490
F	-2.554497	2.203787	-0.202122
F	-3.180734	0.633978	1.154204
O	-0.452090	0.795994	0.901321
H	0.497781	0.812665	0.650751

Table S10. Experimental transition frequencies of conformer **I** of the HFIP-1,4 dioxane complex.

J'	K_a'	K_c'	J''	K_a''	K_c''	$\nu_{\text{obs}}/\text{MHz}$	$\Delta\nu_{\text{obs-calc}}/\text{MHz}$
6	2	5	5	2	4	3831.1300	0.0119
6	3	4	5	3	3	3877.6800	0.0058
6	3	3	5	3	2	3896.3030	-0.0057
4	1	4	3	1	3	2449.1770	0.0053
4	0	4	3	0	3	2518.1270	-0.0065
4	2	3	3	2	2	2566.3050	-0.0046
4	3	1	3	3	0	2582.8290	-0.0058
4	3	2	3	3	1	2580.7500	-0.0061
4	2	2	3	2	1	2618.8270	0.0077
4	1	3	3	1	2	2669.7770	-0.0021
5	0	5	4	0	4	3115.7270	-0.0021
5	2	4	4	2	3	3200.9520	-0.0081
5	3	3	4	3	2	3228.9770	0.0043
5	4	1	4	4	0	3225.7030	0.0095
5	4	2	4	4	1	3225.5510	0.0019
5	3	2	4	3	1	3236.1530	0.0061
5	2	3	4	2	2	3298.4010	-0.0047
5	1	4	4	1	3	3324.3740	-0.0012
6	1	6	5	1	5	3653.2730	0.0348
6	0	6	5	0	5	3702.8570	-0.0033
6	4	2	5	4	1	3875.1790	-0.0050
6	4	3	5	4	2	3874.5360	-0.0028
6	1	5	5	1	4	3968.6130	-0.0056
7	1	7	6	1	6	4249.6760	-0.0099
7	0	7	6	0	6	4285.0520	-0.0010
7	2	6	6	2	5	4456.1000	-0.0049
7	3	4	6	3	3	4565.8530	-0.0018
7	1	6	6	1	5	4599.2500	-0.0053
7	2	5	6	2	4	4667.5490	0.0014
8	1	8	7	1	7	4843.1630	-0.0016
8	0	8	7	0	7	4866.4270	0.0019
8	2	7	7	2	6	5075.4530	-0.0055
8	3	5	7	3	4	5246.5270	-0.0083

8 2 6	7 2 5	5344.5660	0.0001
9 1 9	8 1 8	5434.3770	-0.0038
9 0 9	8 0 8	5448.8250	0.0022
9 2 8	8 2 7	5689.0040	-0.0030
9 3 7	8 3 6	5814.9270	0.0054
9 4 6	8 4 5	5831.6890	0.0036
9 4 5	8 4 4	5845.0250	0.0067
4 4 1	3 3 1	5489.9500	0.0063
4 4 0	3 3 0	5489.6100	-0.0031
5 3 3	4 2 3	5331.2180	-0.0071
5 3 2	4 2 2	5260.8740	-0.0162
5 2 4	4 1 4	4739.1200	0.0140
4 3 2	3 2 2	4668.5560	-0.0060
5 2 3	4 1 3	4362.1930	-0.0043
3 3 0	2 2 0	4010.5950	0.0135
3 3 1	2 2 1	4015.7940	0.0042
4 2 3	3 1 3	3987.3120	-0.0056
4 2 2	3 1 2	3733.5790	0.0083
9 3 6	8 3 5	5937.6880	0.0036
9 1 8	8 1 7	5812.0470	0.0058
8 1 7	7 1 6	5213.7790	-0.0028
8 4 4	7 4 3	5183.5770	-0.0022
8 4 5	7 4 4	5177.8510	-0.0041
8 3 6	7 3 5	5171.9770	-0.0061
7 4 3	6 4 2	4527.4660	0.0014
7 3 5	6 3 4	4525.7780	-0.0031
7 4 4	6 4 3	4525.3480	0.0067
3 1 2	2 1 1	2007.8440	0.0043

Appendix B

Supporting Information for Chapter 4

Rotational Spectroscopy and Ab Initio Calculations of 1-Phenyl-2,2,2-Trifluoroethanol···1,4-Dioxane Complex

Contents:

Table S1. Spectroscopic parameters of the group c) conformers of PhTFE···1,4-dioxane.....	S2
Tables S2-S7. Coordinates of six PhTFE···1,4-dioxane conformers.....	S3-S8
Tables S8-S9. Experimental frequencies of the two PhTFE-1,4 dioxan conformers.....	S9-S15
Figure S1. QTAIM and NCI analyses of three most stable PhTFE-1,4 dioxane conformers.....	S16

Table S1. The relative raw, *ZPE* and *ZPE/BSSE* corrected relative energies and *ZPE/BSSE* corrected binding energies and spectroscopic parameters of the group (c) conformers of the PhTFE···1,4-dioxane complex calculated at the B3LYP-D3(BJ)/def2-TZVP level of theory.^a

Conformer	ΔE	ΔE_0	$\Delta E_{0(BSSE)}$	ΔE_b	<i>A</i>	<i>B</i>	<i>C</i>	μ_a	μ_b	μ_c
<i>g</i> -Ph-dio XVIII	19.6	17.8	17.3	27.6	547	312	248	1.1	-1.5	0.3
<i>g</i> -Ph-dio XIX	21.4	19.0	18.1	24.7	543	273	215	1.0	2.4	0.3
<i>g</i> -Ph-dio XX	23	20.3	19.8	23.2	601	266	218	1.3	-2.1	-0.1
<i>g</i> -Ph-dio XXI	23.2	21.7	21.6	26.0	489	360	269	-1.4	2.1	-0.1
<i>g</i> -Ph-dio XXII	24.5	21.8	20.8	21.9	511	268	200	-0.1	-2.5	0.3
<i>g</i> -Ph-dio XXIII	25.7	22.7	21.9	21.1	539	259	204	-0.5	2.4	-0.2
<i>g</i> -Ph-dio XXIV	26.4	23.3	22.5	20.3	499	304	225	-0.5	2.4	0.0
<i>g</i> -Ph-dio XXV	27.6	24.4	23.9	19.2	609	284	236	-1.6	2.3	-0.4
<i>g</i> -Ph-dio XXVI	29.0	26.1	25.7	18.4	631	279	235	1.3	1.7	0.1

^a ΔE , ΔE_0 , $\Delta E_{0(BSSE)}$ are the relative raw, *ZPE* corrected relative, and both *ZPE* and *BSSE* corrected relative energies in kJ mol^{-1} , respectively. ΔE_b is the both *ZPE* and *BSSE* corrected binding energy in kJ mol^{-1} . *A*, *B*, and *C* are the rotational constants in MHz and μ_g ($g = a, b, c$) are the electric dipole moment components in Debye.

Table S2. DFT coordinates of conformer **I** of the PhTFE···1,4-dioxane complex in its principal inertial axis system at the B3LYP-D3(BJ)/def2-TZVP level of theory.

Atom	<i>a</i> (Å)	<i>b</i> (Å)	<i>c</i> (Å)
C	0.285685	2.681980	1.141277
C	0.485661	3.268057	-0.102757
C	0.126495	2.578433	-1.256189
C	-0.429051	1.308846	-1.167389
C	-0.628125	0.715950	0.077022
C	-0.267910	1.410493	1.227889
H	-0.419664	0.953388	2.198158
C	-1.220583	-0.675534	0.174551
O	-0.840104	-1.526496	-0.872443
H	0.135709	-1.577664	-0.882307
H	-0.963066	-1.098677	1.154946
C	-2.752120	-0.636489	0.161082
F	-3.209968	0.125951	1.177634
F	-3.272967	-1.864474	0.319066
F	-3.245249	-0.129185	-0.979296
H	-0.708123	0.765572	-2.059646
H	0.277085	3.032611	-2.227193
H	0.921757	4.255991	-0.173593
H	0.567191	3.210381	2.042728
O	3.806058	-0.179857	0.769681
C	3.168227	0.433601	-0.346675
H	3.891172	1.122943	-0.783252
C	2.750708	-0.611479	-1.362790
H	2.168961	-0.164023	-2.167639
H	3.632857	-1.106384	-1.785479
O	1.912954	-1.598945	-0.754473
C	2.537492	-2.196059	0.383111
H	1.810527	-2.886545	0.811472
C	2.945951	-1.129387	1.381124
H	3.497155	-1.570620	2.212148
H	2.052441	-0.626161	1.773931
H	3.417620	-2.761736	0.055590
H	2.294765	1.001451	-0.012634

Table S3. DFT coordinates of conformer **II** of the PhTFE···1,4-dioxane complex in its principal inertial axis system at the B3LYP-D3(BJ)/def2-TZVP level of theory.

Atom	<i>a</i> (Å)	<i>b</i> (Å)	<i>c</i> (Å)
C	0.670898	-3.054574	1.024187
C	0.214018	-3.441349	-0.229528
C	0.135808	-2.504398	-1.255460
C	0.506541	-1.186733	-1.027514
C	0.960751	-0.791954	0.230048
C	1.042865	-1.734121	1.250244
H	1.388984	-1.430702	2.230683
C	1.304900	0.658112	0.497549
O	0.353310	1.550155	-0.025670
H	-0.517125	1.293810	0.338887
H	1.432188	0.795276	1.578870
C	2.654547	1.053612	-0.104804
F	3.631116	0.255875	0.377304
F	2.978168	2.318179	0.212955
F	2.677657	0.955710	-1.444543
H	0.433427	-0.452069	-1.817150
H	-0.216267	-2.802201	-2.234770
H	-0.079677	-4.467686	-0.407731
H	0.732578	-3.777323	1.827349
O	-4.168252	0.378733	-0.802790
C	-3.672596	1.683438	-0.538009
H	-4.509404	2.372088	-0.657925
C	-3.107453	1.765893	0.867443
H	-2.644588	2.735434	1.051983
H	-3.901399	1.600196	1.604761
O	-2.085395	0.782066	1.052022
C	-2.573825	-0.535318	0.768786
H	-1.730953	-1.213877	0.881944
C	-3.144709	-0.594525	-0.633710
H	-3.596211	-1.568257	-0.824163
H	-2.344284	-0.427523	-1.364876
H	-3.346737	-0.790766	1.502669
H	-2.892585	1.943697	-1.266240

Table S4. DFT coordinates of conformer **III** of the PhTFE···1,4-dioxane complex in its principal inertial axis system at the B3LYP-D3(BJ)/def2-TZVP level of theory.

Atom	<i>a</i> (Å)	<i>b</i> (Å)	<i>c</i> (Å)
C	-0.276859	-2.872003	-1.099627
C	-0.355674	-3.505085	0.134891
C	-0.681109	-2.768220	1.269232
C	-0.919523	-1.403950	1.171771
C	-0.835128	-0.763493	-0.063026
C	-0.517943	-1.506766	-1.195510
H	-0.452711	-1.013536	-2.157731
C	-1.046740	0.732885	-0.162720
O	-0.509277	1.443304	0.921546
H	0.416049	1.151648	1.038963
H	-0.634475	1.082624	-1.118943
C	-2.532906	1.095394	-0.226401
F	-3.114743	0.491884	-1.285272
F	-2.705891	2.419121	-0.377524
F	-3.205867	0.721201	0.872877
H	-1.157842	-0.823739	2.052241
H	-0.747122	-3.257546	2.232378
H	-0.164981	-4.567542	0.213488
H	-0.025042	-3.438846	-1.986554
O	3.960191	0.491077	-1.044419
C	3.018677	-0.547117	-0.803180
H	3.485111	-1.480285	-1.119172
C	2.644223	-0.606493	0.664372
H	1.853707	-1.333137	0.840998
H	3.521237	-0.869509	1.267024
O	2.144519	0.661790	1.102093
C	3.079105	1.712055	0.845475
H	2.599287	2.640406	1.155435
C	3.445042	1.746526	-0.625973
H	4.221739	2.488359	-0.813518
H	2.558175	2.005164	-1.221145
H	3.976876	1.550979	1.453533
H	2.117844	-0.382611	-1.407333

Table S5. DFT coordinates of conformer **IV** of the PhTFE···1,4-dioxane complex in its principal inertial axis system at the B3LYP-D3(BJ)/def2-TZVP level of theory.

Atom	<i>a</i> (Å)	<i>b</i> (Å)	<i>c</i> (Å)
C	-0.262359	2.724395	-1.049674
C	0.197173	3.308527	0.126699
C	0.150328	2.592331	1.316059
C	-0.353415	1.296638	1.325631
C	-0.810624	0.706483	0.151821
C	-0.761985	1.429771	-1.038605
H	-1.106529	0.966490	-1.952679
C	-1.316704	-0.720376	0.159951
O	-0.836644	-1.485677	-0.915783
H	0.136848	-1.403755	-0.917173
H	-1.060794	-1.177060	1.125401
C	-2.844539	-0.789557	0.097251
F	-3.383822	-0.108171	1.130845
F	-3.278414	-2.057950	0.185967
F	-3.344364	-0.269075	-1.034924
H	-0.388237	0.738167	2.253285
H	0.509036	3.038638	2.234393
H	0.590661	4.316682	0.115234
H	-0.230153	3.280019	-1.978091
O	4.390775	-0.377106	0.482420
C	3.796047	-1.619534	0.828240
H	4.102016	-1.844681	1.850245
C	2.285245	-1.535349	0.727283
H	1.822087	-2.505933	0.906304
H	1.900333	-0.809693	1.453968
O	1.902038	-1.133921	-0.589578
C	2.499786	0.121117	-0.937722
H	2.188890	0.341692	-1.957920
C	4.008013	0.022316	-0.827562
H	4.470087	0.992804	-1.009686
H	4.390382	-0.697579	-1.563595
H	2.118337	0.901936	-0.272718
H	4.167127	-2.411186	0.163461

Table S6. DFT coordinates of conformer **V** of the PhTFE···1,4-dioxane complex in its principal inertial axis system at the B3LYP-D3(BJ)/def2-TZVP level of theory.

Atom	<i>a</i> (Å)	<i>b</i> (Å)	<i>c</i> (Å)
C	-0.113258	-2.866926	0.914039
C	-0.567963	-3.155213	-0.366641
C	-0.389092	-2.227323	-1.387812
C	0.240588	-1.017589	-1.130133
C	0.699893	-0.724022	0.152349
C	0.518126	-1.655029	1.169905
H	0.872494	-1.431115	2.168924
C	1.375946	0.601482	0.436902
O	0.776275	1.687591	-0.218445
H	-0.158080	1.730700	0.064365
H	1.409642	0.754174	1.523724
C	2.845010	0.592366	0.004064
F	3.508221	-0.407428	0.623654
F	3.457798	1.741245	0.332923
F	2.994441	0.417612	-1.318976
H	0.375218	-0.288573	-1.917029
H	-0.743245	-2.447666	-2.386573
H	-1.064078	-4.095602	-0.568126
H	-0.252777	-3.582188	1.714186
O	-3.963540	-0.030592	-0.210706
C	-3.326469	0.772425	-1.194582
H	-4.075603	1.000158	-1.953512
C	-2.791318	2.048276	-0.573652
H	-2.223721	2.634007	-1.296784
H	-3.618246	2.656482	-0.188732
O	-1.895488	1.745419	0.498948
C	-2.508564	0.902870	1.478301
H	-1.738326	0.665114	2.211841
C	-3.055593	-0.357322	0.835807
H	-3.612459	-0.946057	1.565268
H	-2.234544	-0.964614	0.443322
H	-3.314348	1.459220	1.971485
H	-2.505179	0.212952	-1.659566

Table S7. DFT coordinates of conformer **VI** of the PhTFE···1,4-dioxane complex in its principal inertial axis system at the B3LYP-D3(BJ)/def2-TZVP level of theory.

Atom	<i>a</i> (Å)	<i>b</i> (Å)	<i>c</i> (Å)
C	0.534449	2.504216	-1.404127
C	1.246955	3.209440	-0.445134
C	1.007997	2.962038	0.902877
C	0.064143	2.018646	1.279621
C	-0.659135	1.304500	0.321460
C	-0.413503	1.557997	-1.025851
H	-0.953073	1.027335	-1.795026
C	-1.673048	0.300261	0.853110
O	-1.128270	-0.551862	1.826408
H	-0.283850	-0.925291	1.498480
H	-2.480284	0.850277	1.347149
C	-2.387828	-0.533482	-0.215605
F	-3.078209	0.242293	-1.080043
F	-3.266586	-1.375633	0.344029
F	-1.530642	-1.284926	-0.947085
H	-0.115590	1.818803	2.327866
H	1.555666	3.506929	1.661096
H	1.983882	3.943648	-0.743257
H	0.715774	2.683697	-2.455844
O	3.152339	-1.113163	-1.043497
C	1.924481	-1.773995	-1.321536
H	2.119132	-2.479153	-2.130131
C	1.420273	-2.500272	-0.089771
H	0.437357	-2.936204	-0.261469
H	2.123189	-3.291633	0.196170
O	1.277531	-1.587280	1.001196
C	2.494450	-0.888408	1.271609
H	2.272973	-0.172572	2.062645
C	2.992323	-0.185462	0.023899
H	3.969896	0.263644	0.202111
H	2.288723	0.601160	-0.265781
H	3.244030	-1.603522	1.630777
H	1.174159	-1.046869	-1.654554

Table S8. Experimental transition frequencies of conformer **I** of the PhTFE-1,4 dioxane complex.

J'	K_a'	K_c'	J''	K_a''	K_c''	$\nu_{\text{obs}}/\text{MHz}$	$\Delta\nu_{\text{obs-calc}}/\text{MHz}$
4	0	4	3	0	3	2023.4467	-0.0028
4	2	3	3	2	2	2084.9339	-0.0023
4	3	2	3	3	1	2103.8290	-0.0035
4	2	2	3	2	1	2152.1537	-0.0035
4	1	3	3	1	2	2185.3480	0.0010
5	1	5	4	1	4	2447.5310	-0.0010
5	0	5	4	0	4	2493.3910	0.0013
5	2	4	4	2	3	2596.9770	0.0026
3	2	1	2	1	2	2626.2930	0.0008
5	4	2	4	4	1	2629.8060	-0.0032
5	4	1	4	4	0	2630.1500	-0.0014
5	3	3	4	3	2	2632.9740	0.0003
5	3	2	4	3	1	2645.5263	0.0002
5	1	4	4	1	3	2713.5450	0.0015
5	2	3	4	2	2	2716.6260	-0.0034
4	2	3	3	1	2	2861.2830	-0.0027
6	0	6	5	1	5	2881.7400	0.0039
6	1	6	5	1	5	2924.5650	-0.0021
6	0	6	5	0	5	2956.1080	-0.0004
6	2	5	5	2	4	3103.1750	0.0002
3	3	1	2	2	0	3129.1860	0.0022
3	3	0	2	2	1	3137.2030	0.0007
6	5	2	5	5	1	3154.7200	0.0132
6	5	1	5	5	0	3154.7200	-0.0137
6	4	3	5	4	2	3160.7510	0.0031
6	3	4	5	3	3	3161.7790	0.0007
6	4	2	5	4	1	3162.2684	0.0018
6	3	3	5	3	2	3193.6620	-0.0013
4	2	3	3	1	3	3194.9430	-0.0080
6	1	5	5	1	4	3226.9320	0.0002
5	2	4	4	1	3	3272.9130	0.0000
6	2	4	5	2	3	3281.6060	0.0018
7	1	6	6	2	5	3286.3370	0.0007
5	1	4	4	0	4	3386.5980	-0.0165
7	1	7	6	1	6	3398.0830	0.0015
7	0	7	6	0	6	3417.5070	0.0025
5	2	3	4	1	3	3495.9520	-0.0005
7	2	6	6	2	5	3602.8650	0.0016
4	3	2	3	2	1	3636.2180	0.0060
4	3	1	3	2	1	3640.4950	-0.0169
6	2	5	5	1	4	3662.5480	0.0036
4	3	2	3	2	2	3672.3750	-0.0004
4	3	1	3	2	2	3676.6760	0.0007

7 6 2	6 6 1	3679.6260	-0.0026
7 6 1	6 6 0	3679.6260	-0.0045
7 5 3	6 5 2	3685.1710	0.0039
7 5 2	6 5 1	3685.3180	0.0045
7 3 5	6 3 4	3688.5300	0.0044
7 4 3	6 4 2	3698.6620	0.0026
7 1 6	6 1 5	3721.9060	-0.0430
7 3 4	6 3 3	3754.5000	0.0037
5 2 4	4 1 4	3825.7510	-0.0032
7 2 5	6 2 4	3839.1320	-0.0010
8 0 8	7 1 7	3856.7050	-0.0008
8 1 8	7 1 7	3869.0210	-0.0030
8 0 8	7 0 7	3880.1160	0.0022
8 1 7	7 2 6	3881.8590	0.0034
8 1 8	7 0 7	3892.4230	-0.0090
5 2 3	4 1 4	4048.7970	0.0033
6 2 4	5 1 4	4064.0150	0.0017
8 2 7	7 2 6	4095.8040	-0.0010
5 3 2	4 2 2	4133.8800	-0.0008
8 1 7	7 1 6	4198.3860	0.0033
8 7 2	7 7 1	4204.6260	0.0042
8 7 1	7 7 0	4204.6260	0.0040
8 6 3	7 6 2	4209.5510	0.0012
8 3 6	7 3 5	4211.4000	0.0044
8 5 4	7 5 3	4217.7120	0.0007
8 5 3	7 5 2	4218.2920	0.0034
5 3 3	4 2 3	4220.4130	0.0001
8 4 5	7 4 4	4228.1850	-0.0013
5 3 2	4 2 3	4237.2670	0.0018
8 4 4	7 4 3	4241.3000	0.0053
4 4 1	3 3 0	4281.3650	-0.0092
4 4 0	3 3 1	4282.0500	0.0121
8 3 5	7 3 4	4327.1500	0.0001
9 0 9	8 1 8	4331.9510	-0.0003
9 1 9	8 1 8	4338.2550	0.0001
9 0 9	8 0 8	4344.2700	0.0005
9 1 9	8 0 8	4350.5720	-0.0011
8 2 6	7 2 5	4383.9520	-0.0015
8 2 7	7 1 6	4412.3270	-0.0050
9 1 8	8 2 7	4447.0960	0.0013
6 2 5	5 1 5	4481.3940	-0.0030
6 3 4	5 2 3	4562.1780	0.0006
9 2 8	8 2 7	4582.2760	-0.0030
6 3 3	5 2 3	4610.9140	-0.0007
9 1 8	8 1 7	4661.0450	0.0010

7 2 5	6 1 5	4676.2220	0.0075
9 3 7	8 3 6	4728.7610	0.0015
9 8 1	8 8 0	4729.6620	0.0011
9 7 3	8 7 2	4734.1560	0.0017
9 7 2	8 7 1	4734.1560	0.0008
9 6 4	8 6 3	4741.1560	-0.0326
9 6 3	8 6 2	4741.2780	0.0327
9 5 5	8 5 4	4752.4760	-0.0021
9 4 6	8 4 5	4763.1360	0.0058
6 3 4	5 2 4	4785.2160	-0.0008
9 4 5	8 4 4	4792.8510	0.0046
9 2 8	8 1 7	4796.2310	0.0027
10 0 10	9 1 9	4803.2770	0.0017
5 4 2	4 3 1	4803.6780	0.0063
5 4 1	4 3 1	4804.0610	0.0041
10 1 10	9 1 9	4806.4350	0.0021
5 4 2	4 3 2	4807.9770	0.0055
5 4 1	4 3 2	4808.3610	0.0042
10 0 10	9 0 9	4809.5800	0.0010
6 3 3	5 2 4	4833.9530	-0.0012
9 3 6	8 3 5	4905.5270	-0.0005
9 2 7	8 2 6	4912.2760	0.0010
7 3 5	6 2 4	4969.1040	0.0052
0 1 9	9 2 8	4982.3250	-0.0020
10 2 9	9 2 8	5063.0500	0.0087
10 1 9	9 1 8	5117.5160	0.0048
0 2 9	9 1 8	5198.2170	-0.0086
10 3 8	9 3 7	5239.3860	0.0023
10 9 2	9 9 1	5254.7350	0.0066
10 9 1	9 9 0	5254.7350	0.0066
10 8 2	9 8 1	5258.9140	0.0014
10 8 3	9 8 2	5258.9140	0.0014
10 7 3	9 7 2	5265.1020	-0.0016
10 7 4	9 7 3	5265.1020	0.0034
11 1 11	10 1 10	5274.0040	0.0005
10 6 5	9 6 4	5274.7550	-0.0044
10 6 4	9 6 3	5274.9700	0.0014
11 0 11	10 0 10	5275.6120	0.0061
11 1 11	10 0 10	5277.1540	-0.0070
10 5 6	9 5 5	5289.4050	-0.0020
10 5 5	9 5 4	5294.3930	0.0037
10 4 7	9 4 6	5297.0410	0.0050
6 4 3	5 3 2	5318.8970	0.0036
6 4 3	5 3 3	5335.7370	-0.0087
6 4 2	5 3 3	5337.6540	0.0043

8 2 6	7 1 6	5338.2150	-0.0041
8 3 6	7 2 5	5341.3690	0.0076
10 4 6	9 4 5	5356.1190	-0.0014
7 3 5	6 2 5	5370.5680	0.0004
10 2 8	9 2 7	5420.8560	0.0000
5 5 1	4 4 0	5430.0510	-0.0086
5 5 0	4 4 0	5430.0510	-0.0113
5 5 0	4 4 1	5430.1120	0.0066
5 5 1	4 4 1	5430.1120	0.0093
10 3 7	9 3 6	5480.4140	0.0013
7 3 4	6 2 5	5485.2790	0.0033
11 2 10	10 2 9	5539.1670	0.0014
11 1 10	10 1 9	5573.7860	-0.0011
11 2 10	10 1 9	5619.8800	0.0001
9 3 7	8 2 6	5686.1600	-0.0073
12 0 12	11 1 11	5740.4820	-0.0042
12 1 12	11 1 11	5741.2400	-0.0017
12 0 12	11 0 11	5742.0450	0.0037
11 3 9	10 3 8	5742.5560	0.0044
12 1 12	11 0 11	5742.7980	0.0012
11 10 1	10 10 0	5779.8140	-0.0002
11 9 2	10 9 1	5783.7520	-0.0163
11 8 4	10 8 3	5789.3540	-0.0011
11 8 3	10 8 2	5789.3540	-0.0015
11 7 5	10 7 4	5797.6360	0.0096
11 7 4	10 7 3	5797.6360	-0.0111
11 6 6	10 6 5	5810.4500	0.0014
11 6 5	10 6 4	5811.1030	-0.0011
11 4 8	10 4 7	5828.1070	0.0069
11 5 7	10 5 6	5828.1070	-0.0188
11 5 6	10 5 5	5840.0440	-0.0040
7 4 4	6 3 4	5867.6840	0.0033
11 2 9	10 2 8	5908.0030	0.0010
6 5 2	5 4 1	5954.6150	0.0000
6 5 1	5 4 1	5954.6150	-0.0296
6 5 1	5 4 2	5955.0260	-0.0039
6 5 2	5 4 2	5955.0260	0.0257
12 1 11	11 2 10	5986.3920	0.0016

Table S9. Experimental transition frequencies of conformer **II** of the PhTFE-1,4 dioxane complex.

J'	K_a'	K_c'	J''	K_a''	K_c''	$\nu_{\text{obs}}/\text{MHz}$	$\Delta\nu_{\text{obs-calc}}/\text{MHz}$
4	1	3	3	1	2	2051.5780	0.0035
5	1	5	4	1	4	2248.6740	-0.0172
5	0	5	4	0	4	2292.3650	-0.0159
5	1	5	4	0	4	2354.1350	-0.0093
5	1	4	4	1	3	2541.2340	0.0052
5	2	3	4	2	2	2558.8160	0.0487
6	0	6	5	1	5	2650.1420	0.0004
6	1	6	5	1	5	2683.7570	-0.0074
6	0	6	5	0	5	2711.8960	-0.0090
6	2	5	5	2	4	2882.3710	-0.0085
6	3	4	5	3	3	2953.5450	0.0140
6	4	3	5	4	2	2953.9420	-0.0045
6	4	2	5	4	1	2956.3410	0.0124
6	3	3	5	3	2	2997.2360	0.0171
6	1	5	5	1	4	3012.0080	0.0043
3	3	0	2	2	1	3017.5570	-0.0053
5	2	4	4	1	3	3055.7400	-0.0089
6	2	4	5	2	3	3091.3950	0.0117
7	0	7	6	1	6	3097.6890	0.0006
7	1	7	6	1	6	3115.0560	-0.0083
7	0	7	6	0	6	3131.3050	-0.0062
7	1	7	6	0	6	3148.6810	-0.0061
4	2	2	3	1	3	3189.7600	-0.0311
5	2	3	4	1	3	3325.8800	0.0001
7	2	6	6	2	5	3341.2840	-0.0030
6	2	5	5	1	4	3396.9020	0.0024
7	6	1	6	6	0	3436.6270	0.0089
7	6	2	6	6	1	3436.6270	0.0127
7	5	3	6	5	2	3443.5210	-0.0037
7	5	2	6	5	1	3443.7960	0.0126
7	3	5	6	3	4	3444.1420	0.0082
7	4	4	6	4	3	3453.5980	0.0042
7	1	6	6	1	5	3460.4390	-0.0103
7	4	3	6	4	2	3461.3150	0.0125
4	3	2	3	2	1	3475.1680	0.0019
4	3	2	3	2	2	3520.0530	0.0074
4	3	1	3	2	2	3526.0720	0.0084
7	3	4	6	3	3	3532.4740	0.0133
8	0	8	7	1	7	3535.1110	-0.0011
8	1	8	7	1	7	3543.7580	-0.0066
7	2	5	6	2	4	3612.7690	0.0084
8	1	7	7	2	6	3622.9470	0.0195
5	2	4	4	1	4	3669.6890	0.0000

8 2 7	7 2 6	3792.2710	-0.0021
6 2 4	5 1 4	3876.0440	0.0096
8 1 7	7 1 6	3888.6580	-0.0031
5 3 3	4 2 2	3911.1630	-0.0073
8 3 6	7 3 5	3929.3270	0.0023
5 3 2	4 2 2	3934.6240	-0.0009
12 7 5	12 6 6	3935.8690	0.0038
8 5 4	7 5 3	3943.0140	0.0025
8 5 3	7 5 2	3944.0310	0.0040
8 4 5	7 4 4	3954.6130	0.0018
9 0 9	8 1 8	3966.6410	-0.0077
9 1 9	8 1 8	3970.8390	-0.0018
8 4 4	7 4 3	3974.8270	0.0045
9 0 9	8 0 8	3975.2960	-0.0052
9 1 9	8 0 8	3979.4780	-0.0153
6 1 5	5 0 5	3980.2880	0.0432
8 2 7	7 1 6	4057.9950	-0.0117
5 3 2	4 2 3	4061.6190	0.0251
8 3 5	7 3 4	4079.3820	0.0032
8 2 6	7 2 5	4117.2450	-0.0036
4 4 1	3 3 0	4119.3020	-0.0014
4 4 0	3 3 1	4120.2280	-0.0142
9 2 8	8 2 7	4235.9650	0.0006
9 1 8	8 1 7	4304.7220	-0.0042
6 3 3	5 2 3	4373.0750	-0.0016
10 0 10	9 1 9	4394.9990	0.0070
10 1 10	9 1 9	4396.9890	0.0081
10 0 10	9 0 9	4399.1800	-0.0042
10 1 10	9 0 9	4401.1730	0.0000
9 7 3	8 7 2	4422.5220	0.0070
9 7 2	8 7 1	4422.5220	0.0049
9 6 4	8 6 3	4431.3340	0.0068
9 6 3	8 6 2	4431.4300	-0.0095
9 5 5	8 5 4	4445.1320	-0.0045
9 5 4	8 5 3	4448.3430	-0.0034
9 4 6	8 4 5	4455.4210	-0.0047
7 2 5	6 1 5	4476.8170	0.0257
9 4 5	8 4 4	4500.4410	-0.0058
6 3 4	5 2 4	4576.0530	-0.0121
9 2 7	8 2 6	4600.4150	-0.0112
5 4 2	4 3 1	4605.7050	-0.0019
5 4 1	4 3 1	4606.3250	0.0114
5 4 2	4 3 2	4611.7250	0.0001
5 4 1	4 3 2	4612.3290	-0.0026
10 1 9	9 2 8	4617.0500	-0.0043

9 3 6	8 3 5	4628.1270	0.0067
6 3 3	5 2 4	4643.2220	0.0144
7 3 5	6 2 4	4658.6590	-0.0256
10 2 9	9 2 8	4673.5310	-0.0065
10 1 9	9 1 8	4717.6350	-0.0031
10 2 9	9 1 8	4774.1220	0.0007
11 0 11	10 1 10	4821.6930	0.0060
11 1 11	10 1 10	4822.6230	0.0080
11 0 11	10 0 10	4823.6830	0.0071
11 1 11	10 0 10	4824.6140	0.0102
10 3 8	9 3 7	4876.6910	0.0031
10 7 4	9 7 3	4920.0890	0.0022
10 7 3	9 7 2	4920.0890	-0.0088
10 6 5	9 6 4	4932.1660	-0.0004
10 6 4	9 6 3	4932.5730	-0.0061
10 5 6	9 5 5	4949.6520	0.0010
10 4 7	9 4 6	4953.9280	-0.0011
10 5 5	9 5 4	4958.2810	-0.0045
8 3 6	7 2 5	4975.2480	-0.0007
11 2 9	10 3 8	5010.3490	-0.0119
10 4 6	9 4 5	5041.0210	-0.0074
10 2 8	9 2 7	5058.9170	-0.0120
6 4 3	5 3 2	5082.4720	-0.0022
6 4 2	5 3 2	5085.4550	-0.0080
6 4 3	5 3 3	5105.9430	0.0143
11 2 10	10 2 9	5106.4370	-0.0024
6 4 2	5 3 3	5108.9170	-0.0005
11 1 10	10 1 9	5132.5340	0.0011
8 2 6	7 1 6	5133.6110	0.0204
7 3 5	6 2 5	5137.8260	0.0066
10 3 7	9 3 6	5167.3280	-0.0152
5 5 1	4 4 0	5226.8270	-0.0133
5 5 0	4 4 1	5226.9220	0.0089
12 0 12	11 1 11	5247.5760	0.0139
12 1 12	11 0 11	5248.9280	0.0108
11 3 9	10 3 8	5337.1220	0.0026
11 8 3	10 8 2	5409.2590	-0.0077
11 8 4	10 8 3	5409.2590	-0.0067
11 7 5	10 7 4	5419.6500	-0.0018
11 7 4	10 7 3	5419.7020	0.0042
11 6 6	10 6 5	5435.6010	-0.0071
11 6 5	10 6 4	5436.8790	-0.0150
11 4 8	10 4 7	5447.7860	-0.0103
11 5 7	10 5 6	5455.8050	-0.0134
11 5 6	10 5 5	5476.1960	-0.0138

11 2 9	10 2 8	5492.9420	-0.0072
12 2 11	11 2 10	5536.0880	0.0050
7 4 4	6 3 3	5538.8480	-0.0010
12 1 11	11 1 10	5550.6520	0.0033
12 2 11	11 1 10	5566.4770	0.0043
11 4 7	10 4 6	5595.5720	-0.0251
7 4 3	6 3 4	5616.6970	0.0080
13 1 13	12 1 12	5673.2650	0.0302
13 0 13	12 0 12	5673.4960	0.0285
11 3 8	10 3 7	5688.6920	-0.0259
6 5 2	5 4 1	5716.3150	-0.0205
6 5 1	5 4 2	5717.0111	0.0165
12 10 2	11 10 1	5892.2870	0.0357
12 9 3	11 9 2	5898.7150	-0.0077
12 2 10	11 2 9	5908.6070	-0.0070
12 4 9	11 4 8	5934.8520	-0.0125
12 6 7	11 6 6	5941.6990	-0.0108
12 6 6	11 6 5	5945.2020	-0.0230
13 1 12	12 2 11	5955.6070	0.0012
8 4 5	7 3 4	5960.9920	-0.0075
12 5 8	11 5 7	5962.2840	-0.0284
13 2 12	12 2 11	5963.6580	0.0216
13 1 12	12 1 11	5971.4430	0.0132

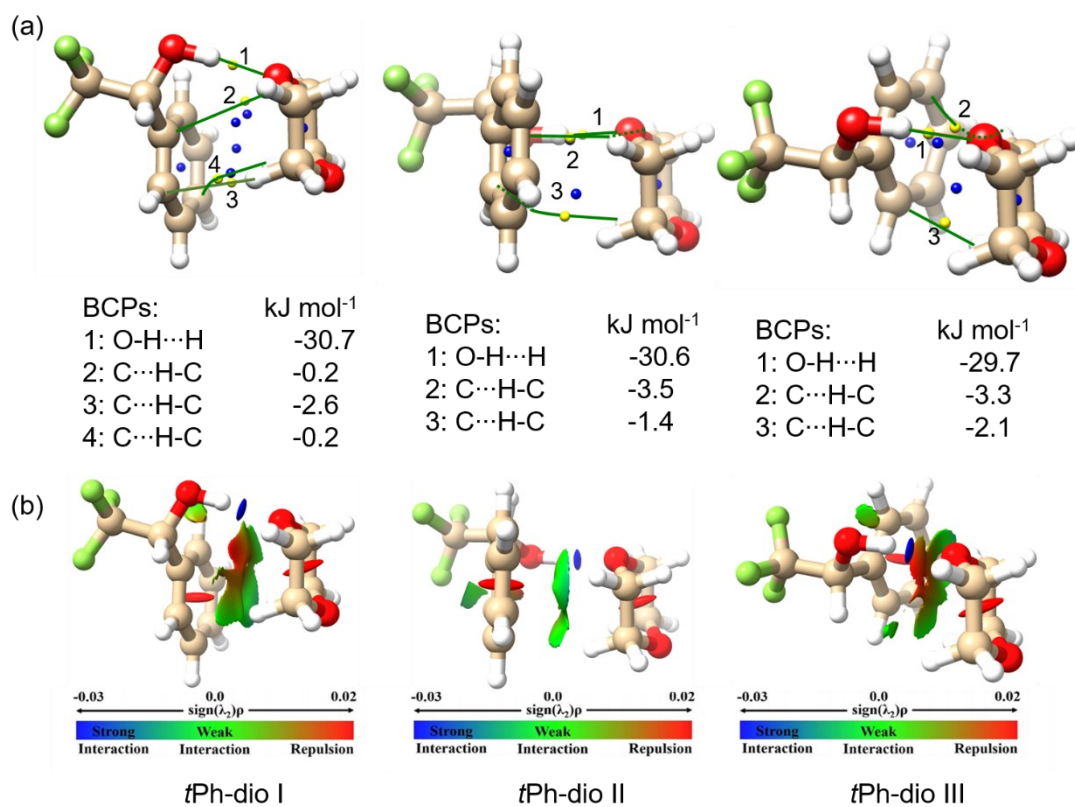


Figure S1. (a) The QTAIM analyses of *tPh-dio I*, *tPh-dio II* and *tPh-dio III*. Yellow dots represent the bond critical points, orange lines represent the corresponding bond paths, and yellow dots represent ring critical points. The associated bond energies are also listed. (b) The corresponding NCI isosurfaces of the three most stable PhTFE...1,4-dioxane conformers.